Bralower, T.J., Premoli Silva, I., and Malone, M.J. (Eds.)
Proceedings of the Ocean Drilling Program, Scientific Results Volume 198

16. Sedimentology, Petrology, and Volcanology of the Lower Aptian Oceanic Anoxic Event (OAE1a), Shatsky Rise, North-Central Pacific Ocean[1]

Kathleen M. Marsaglia[2]

ABSTRACT

This petrological study of the lower Aptian Oceanic Anoxic Event (OAE1a) focused on the nature of the organic-rich interval as well as the tuffaceous units above and below it. The volcaniclastic debris deposited just prior to the OAE1a is consistent with reactivation of volcanic centers across the Shatsky Rise, concurrent with volcanism on the Ontong Java Plateau. This reactivation may have been responsible for the sub-OAE1a unconformity. Soon after this volcanic pulse, anomalous amounts of organic matter accumulated on the rise, forming a black shale horizon. The complex textures in the organic-rich intervals suggest a history of periodic anoxia, overprinted by bioturbation. Components include pellets, radiolarians, and fish debris. The presence of carbonate-cemented radiolarite under the OAE1a intervals suggests that there has been large-scale remobilization of carbonate in the system, which in turn may explain the absence of calcareous microfossils in the section. The volcanic debris in the overlying tuffaceous interval differs in that it is significantly epiclastic and glauconitic. It was likely derived from an emergent volcanic edifice.

[1]Marsaglia, K.M., 2005. Sedimentology, petrology, and volcanology of the lower Aptian Oceanic Anoxic Event (OAE1a), Shatsky Rise, north-central Pacific Ocean. *In* Bralower, T.J., Premoli Silva, I., and Malone, M.J. (Eds.), *Proc. ODP, Sci. Results,* 198, 1–31 [Online]. Available from World Wide Web: <http://www-odp.tamu.edu/publications/198_SR/VOLUME/CHAPTERS/109.PDF>. [Cited YYYY-MM-DD]
[2] Department of Geological Sciences, California State University Northridge, 18111 Nordhoff Street, Northridge CA 91330-8266, USA.
kathie.marsaglia@csun.edu

Initial receipt: 2 March 2004
Acceptance: 29 December 2004
Web publication: 6 July 2005
Ms 198SR-109

INTRODUCTION

The main objective of Ocean Drilling Program (ODP) Leg 198 was to examine the sedimentary record of several ancient "greenhouse" climate events (Bralower, Premoli Silva, Malone, et al., 2002). These events include the early Aptian Oceanic Anoxic Event (OAE1a) or "Selli" interval that was deposited over a period of ~0.6 m.y. (Bralower et al., 1993). This Cretaceous black shale has been found in deep marine sections around the globe, from Italy to the Pacific Ocean Basin (e.g., Sliter, 1989; Coccioni et al., 1992; Bralower et al., 1993, 1994). Oceanic anoxia in the OAE1a interval is manifested by enhanced preservation of organic carbon and significant biotic changes (e.g., Premoli Silva et al., 1999; Leckie et al., 2002). It is linked to high fertility characterized by oligotrophic conditions and poorly oxygenated bottom waters (Coccioni et al., 1992). Some workers link the enhancement of preservation to ocean bottom water stagnation and anoxia (e.g., Bralower and Thierstein, 1984), whereas others attribute the preservation to enhanced productivity (e.g., Pedersen and Calvert, 1990; Hochuli et al., 1999). Bralower et al. (1993) suggest that OAE1a represents a condensed section formed during a period of rapidly rising sea level linked to increased rates of seafloor spreading and anomalous midplate volcanism (e.g., Larson, 1991a, 1991b; Tarduno et al., 1991; Arthur et al., 1991). It is therefore not surprising that cores and outcrops that contain the OAE1a horizon often contain altered volcanic tuffs (e.g., Sliter, 1989, 1999). Data and interpretations about this interval are summarized in several publications (e.g., Bralower et al., 1994; Larson and Erba, 1999; Leckie et al., 2002).

Prior drilling on the Shatsky Rise encountered the OAE1a horizon, but recovery was poor (Site 305; Larson, Moberly, et al., 1975). Recovery of this horizon was better during Leg 198 (Fig. **F1**), particularly near the apex of the Northern High in Cores 198-1207B-43R and 44R (Bralower, Premoli Silva, Malone, et al., 2002). The OAE1a interval was also partly recovered in Cores 198-1213B-8R and 198-1214A-23R on the southern flanks of the Southern High. Gamma and natural uranium logs at Sites 1207 and 1213 suggest that 50% to 30%, respectively, of the OAE1a interval was recovered at these sites (Bralower, Premoli Silva, Malone, et al., 2002). Biostratigraphic and organic carbon analyses suggests that the apex of the OAE1a was at least partly recovered in the sedimentary sections at Sites 1207 and 1213 but was likely missed at Site 1214 (Bralower, Premoli Silva, Malone, et al., 2002). For these reasons, the Site 1207 and 1213 records are emphasized in this discussion.

Given shipboard time constraints, only cursory descriptions of the OAE1a intervals were possible during Leg 198. The goal of this study was to characterize the sedimentology and sedimentary petrology of the OAE1a interval, particularly the organic-rich and volcaniclastic facies. It is important to relate this section to other circum-Pacific occurrences. Deep Sea Drilling Project (DSDP) Site 463 (Fig. **F2**) was chosen as a comparator because a nearly complete section of the OAE1a interval that is both organic rich and tuffaceous was recovered at that site (Shipboard Scientific Party, 1981). Although there have been many geochemical studies of black shales, their petrographic study has been limited (e.g., Schieber, 2003). Results presented here are meant to complement other postcruise geochemical and biostratigraphic (e.g., **Bown,** this volume) studies with the ultimate goal of refining the model for OAE1a formation.

F1. Location map for Leg 198 sites on the Shatsky Rise, p. 16.

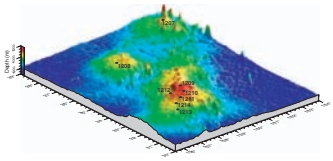

F2. Location of topographic highs in the western Pacific, p. 17

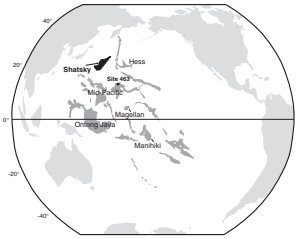

METHODS

Sampling of the OAE1a intervals for this study occurred postcruise at the Gulf Coast Core Repository at Texas A&M University (TAMU) in College Station, Texas, prior to sampling by other shipboard scientists. Therefore, sample intervals were chosen to maximize coverage of the lithologies tentatively differentiated via shipboard core descriptions while minimizing sample volume across critical organic-rich sections. Detailed visual core descriptions (VCDs) of the OAE1a intervals (Cores 198-1207B-43R and 44R, 198-1213B-8R, and 198-1214A-23R) were produced shipboard. These were used as sampling references at TAMU. Section 198-1214A-23R-1 was described in more detail during the sampling process. Representative samples of the various lithologies were selected for thin section preparation, including fragments of chert, organic-rich shale, chalk/limestone, and tuff. There were 36 samples selected, 21 from Cores 198-1207B-43R and 44R, 9 from Core 198-1213B-8R, and 6 from Core 198-1214A-23R (Fig. **F3;** Table **T1**).

Samples from DSDP Site 463 in the Mid-Pacific Mountains were also collected for this study from cores stored at the DSDP West Coast Repository at Scripps Institution of Oceanography in La Jolla, California (Table **T2**). Shipboard descriptions of these cores suggested that the OAE1a interval at Site 463 contained a significant amount of ash. Based on these published descriptions, 17 samples were chosen over a ~24 m interval (604.69–628.27 meters below seafloor [mbsf]).

Billets trimmed from the 53 samples were impregnated with blue-dyed epoxy for porosity recognition prior to preparation of standard petrographic thin sections. Detailed petrographic descriptions were performed on these thin sections (Table **T1**). Categories included biogenic (nannofossils, foraminifers, radiolarians, fish debris, and organic matter), volcanic (plagioclase crystals and altered vitric and microlitic fragments), and matrix components, as well as authigenic phases and porosity. The matrix often consisted of microporous mixtures of clay minerals, silt with authigenic pyrite, zeolites, carbonate, opal-CT, and quartz (chalcedony). Diagenetic phenomena were documented (e.g., replacement of radiolarians by pyrite or calcite, replacement of foraminifers by silica, cementation, and secondary porosity). The presence of lamination and intensity of bioturbation were also noted.

Pristine fragments of 19 representative samples from Leg 198 were selected for X-ray diffraction (XRD) analyses (Table **T2**). Both bulk and clay mineral separates were analyzed by K-T Geoservices, Dallas, Texas, who first disaggregated and split each sample. One-half of each sample was powdered and then pressure packed into an aluminum mount for random whole-rock analysis. The second half was ultrasonically dispersed and then centrifugally size fractionated to concentrate the <4 µm (clay-sized) fraction. Oriented mounts were prepared using vacuum-deposited membranes on glass slides. The slides were glycolated prior to analysis with a Rigaku automated powder diffractometer. Scans were conducted from 2° to 60°θ at a rate of 1°/min for the random mount, and 2° to 50°θ at a rate of 1.5°/min for the glycolated <4 µm fraction mount. Interpretations of mixed-layer clay ordering and expandability were performed by K-T Geoservices using the NEWMOD program created by R.C. Reynolds. Whole-rock mineral proportions were semiquantitatively determined from integrated peak areas (derived from peak-decomposition/profile-fitting methods), empirical reference intensity ratio (RIR) factors and, in the case of the phyllosilicates (clay and mica),

F3. OAE1a core sections and sample intervals, p. 18.

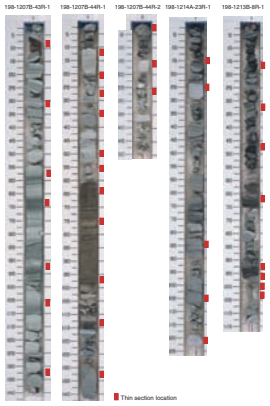

T1. Petrographic summary of thin sections, p. 24.

T2. XRD bulk and clay fraction mineralogy, p. 30.

the combined {00l} and {hkl} clay mineral reflections. The clay-fraction samples were analyzed in a similar manner, also using calculated RIR factor and comparison with simulated diffraction profiles generated by NEWMOD.

RESULTS

Petrography of Leg 198 Samples

Thin section descriptions (Table T1) indicate that the samples range from chert to porcellanite to limestone/chalk, with variable amounts of volcanic and biogenic components. Radiolarians and nannofossils are most important, with lesser foraminifers, ostracodes, and fish debris. Fine matrix mineral proportions are also estimated. Nannofossil chalk/limestone, porcellanite, and chert are similar in appearance to the samples described from underlying and overlying units in the Leg 198 *Initial Reports* (see descriptions and photomicrographs in Bralower, Premoli Silva, Malone, et al., 2002). These shipboard samples were not impregnated with blue epoxy, however, so porosity relationships are better defined here. Primary interparticle, intraparticle, and matrix porosity are present, but these have been affected by recrystallization of the matrix or by precipitation of authigenic phases (e.g., infilled). The distribution of porosity can be seen in the blue hues of the scanned thin sections in Figure F4. This series of thin sections spans the OAE1a interval in Hole 1207B. The altered tuff beds are particularly porous (Fig. F5) in contrast to the organic-rich shales (Figs. F6, F7).

The main authigenic phases are various forms of silica (opal-CT and chalcedony), carbonate, zeolites, pyrite, and gypsum; these occur as cements, grain replacements, and matrix replacements. Secondary porosity arises from the dissolution of biogenic debris, particularly radiolarians and volcanic debris (glass and feldspar). None of the volcanic glass remains; it has either been dissolved (more common) or replaced by authigenic phases such as zeolites (Figs. F5, F6). Locally, opal-CT is also dissolved, forming secondary porosity. Textural relationships suggest that the opal-CT and pyrite routinely preceded precipitation of carbonate (less common), all of which preceded precipitation of chalcedony. Zeolite cements in volcaniclastic intervals appear to postdate all of the above (Figs. F5, F6). Most samples exhibit slight to moderate bioturbation (Figs. F4, F7), but it should be noted that homogeneous samples may be structureless because of thorough bioturbation. Many of the samples are laminated. Thin sections of the organic-rich intervals show what appear to be intact fish remains, as well as fragments (Fig. F6). Foraminifers, even silicified or ghost (dissolved) specimens, are notably absent in the organic-rich intervals. Authigenic calcite is concentrated just below the organic-rich intervals where there are spectacular thin beds of calcite-cemented radiolarite (Fig. F7).

There is no evidence for terrestrial organic matter in the thin sections produced from the OAE1a interval at Sites 1207, 1213, and 1214; however, the thin sections show a variety of textures for the organic matter. The organic matter locally has a globular (Fig. F6) texture (sapropellic algal matter). Where laminae are developed they are first irregular and discontinuous (wispy) (Fig. F7) and grade upward into more continuous laminae, particularly at the top of the OAE1a interval in Hole 1207B (Fig. F6).

F4. OAE1a interval in Hole 1207B, p. 19.

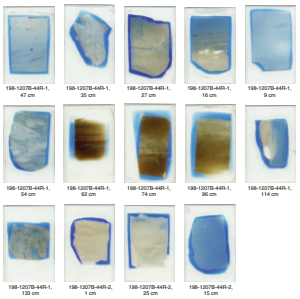

F5. Core 198-1207B-43R photographs, p. 20.

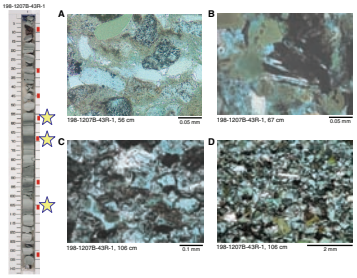

F6. Core 198-1207B-44R photographs, p. 21.

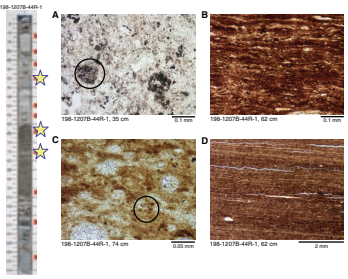

F7. Core 198-1213B-8R photographs, p. 22

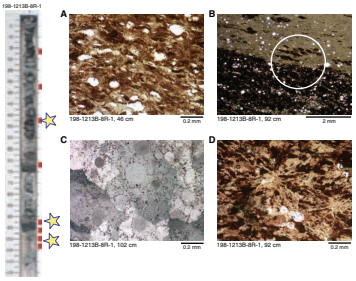

Petrography of Site 463 Samples

DSDP Site 463 was selected for comparison because it was described as containing volcanic ash and organic-rich intervals in the lower Aptian section (Dean et al., 1984). Although a nearly intact section of the OAE1a interval was recovered at Site 463, the working half of the core has been heavily sampled for shipboard and postcruise studies. Seventeen samples were taken spanning the OAE1a (Table T1): five above the organic horizons in Sections 62-463-69R-1 and 70R-1, two within the organic horizons from Sections 70R-2 and 70R-3, and nine below the organic horizons from Sections 70R-7 and 70R-CC and Core 71R. From shipboard descriptions, all had the potential to be ash bearing. However, thin sections produced from these samples indicate most of the samples (11 out of 17) (Table T1) are porcellanite, chalk, and shale, with a few organic-rich shales. Only four samples were tuffaceous, two from above and two from directly below the main organic-rich interval. The textures in the volcanic debris include blocky to moderately vesicular glass altered to zeolites and microlitic volcanic fragments (Fig. F7).

X-Ray Diffraction Data for Leg 198 Samples

Mineral percentages for the 19 samples analyzed are presented in Table T2. The mineral assemblage is dominated by silica phases (quartz and opal-CT), calcite, zeolite (clinoptilolite/heulandite), and phyllosilicates according to the lithology or mix of lithologies present in the sample (e.g., limestone, shale, tuff, porcellanite, and chert). Other important minerals are plagioclase, pyrite, and marcasite, with rare to trace amounts of K-feldspar, halite, and gypsum. The phyllosilicate fraction is mainly randomly ordered mixed-layered illite-smectite with 80%–90% smectite layers and illite/mica. This mineral group includes the petrographically defined glauconite minerals. Traces of kaolinite and chlorite are also present. Although what appeared to be unaltered (isotropic) radiolarians are present, opal-A was not detected in the diffractograms. Clinoptilolite and heulandite are virtually indistinguishable using X-ray diffraction techniques, but the morphology of the zeolite crystals in thin sections of the Leg 198 samples suggests that they are clinoptilolite.

None of the samples from Site 463 were subjected to XRD analysis in this study. However, XRD analyses by several workers (Vallier and Jefferson, 1981; Hein and Vanek, 1981; Mélières et al., 1981; Nagel and Schumann, 1981; Rateev et al., 1981) showed the ash intervals at Site 463 to be mainly composed of montmorillonitic/smectitic and illitic clay minerals, with some siderite. Nagel and Schumann (1981) define tuffaceous intervals by the presence of pyrite, clinoptilolite, and opal-CT.

DISCUSSION

Depositional Setting of the OAE1a Interval on the Shatsky Rise and across the Pacific

During deposition of the OAE1a interval, the Shatsky Rise was likely an isolated submarine high in the equatorial region of the central Pacific. Benthic foraminiferal evidence suggests that Sites 1207, 1213, and 1214 on the Shatsky Rise lay at middle to lower bathyal depths (500–2000 m) during the Aptian (Bralower, Premoli Silva, Malone, et al.,

2002). Therefore, of the depositional processes associated with black shale accumulation summarized by Stow et al. (2001), pelagic settling was perhaps the most important. Pelagic settling would have likely taken the form of pellets created by zooplankton in highly productive surface waters (Stow et al., 2001). Lamination within these sediments could be attributed to bacterial mat development, bottom current activity, or perhaps planar burrowing (pseudolamination, as described in Schieber, 2003). What appear to be whole fish remains in the organic-rich intervals support the idea that bottom waters were poorly oxygenated.

Larson and Erba (1999) argue that there should be an increase in carbonate dissolution with the onset of OAE1a. Bralower et al. (1993) suggest that low carbonate contents of OAE sections as reported in Tethyan (Coccioni et al., 1992; Premoli Silva et al., 1999) and Mid-Pacific Mountain (e.g., Dean et al., 1981) sections are likely related to primary productivity, rather than a secondary byproduct of diagenetic dissolution associated with organic matter oxidation. The radiolarian sparite observed below the OAE1a interval at Site 1207 and also at Site 1214 (Table **T1**) suggests there may have been significant carbonate mobilization in the section. The expanded texture and beautiful preservation of delicate spiny radiolarian tests encased in spar (Fig. **F7**) suggest calcite precipitation must have been a very early phenomenon, prior to sediment compaction. Volume estimates of 94% calcite from XRD data for one sample (Table **T2**) attest to the original high intraparticle (within radiolarians) and interparticle porosity prior to cementation (Fig. **F7**). It is unclear if this calcite was derived from the dissolution of calcareous microfossils in the overlying organic interval or if carbonate directly precipitated near the sediment/water interface prior to the OAE1a. As stated above, no petrographic evidence for foraminifers was observed within the OAE1a organic-rich intervals, not even ghosts.

Authigenic carbonate is also present at Site 463. Thin sections prepared from the Site 463 cores for this study show significant amounts of authigenic Fe stained carbonate (calcite according to Dean et al., 1984), but as matrix replacement rather than sparry cements. Differential diagenesis across the OAE1a intervals at both Site 463 and the Shatsky sites may have contributed to the higher recovery rates compared to units above and below.

Other evidence for the depositional environment of the OAE1a interval comes from the nature of the organic-rich intervals. Most of the organic matter in organic-rich intervals in the Pacific is thought to be algal or bacterial with little input from terrestrial sources (Dean et al., 1984). Shipboard analyses of the OAE1a intervals showed them to be composed of Type I organic matter of algal and bacterial origins, including evidence for some produced by cyanobacteria and haptophytes (e.g., coccoliths) (Bralower, Premoli Silva, Malone, et al., 2002). The latter indicate production of at least some of the organic matter in the photic zone. Shipboard scientists (Bralower, Premoli Silva, Malone, et al., 2002) argued that deposition as microbial mats in highly disoxic or anoxic conditions were needed to explain the nature of the bacterial organic matter, the anomalously high percentage of organic matter, and the overall excellent preservation of the organic compounds.

Shipboard scientists noted in their core descriptions that the organic-rich shales at Site 1213 differed from those at Site 1207 in that the Site 1213 samples showed no evidence for lamination and they were moderately to intensely bioturbated (Fig. **F7**). This could be a function of preferential recovery given the moderate recovery rates (50% and 30%,

as mentioned earlier). Where intact, the organic-rich shales have a gradational base (over several centimeters) but an abrupt top. The presence of bioturbation suggests that oxygen levels were not sufficiently low to completely inhibit benthic activity. Even so, total organic carbon (TOC) values ranged up to ~25 wt% in the Site 1213 core fragments.

The petrographic observations made across the well-developed OAE1a intervals in Sections 198-1207B-44R-1 and 198-1213B-8R-1 indicate that often the organic matter has a more globular texture (sapropellic algal matter) that progressively becomes more laminated upsection. This likely represents the onset of organic matter accumulation and the resultant development of bacteria colonies on the sediment surface. These laminae are first irregular and discontinuous (wispy) (e.g., Fig. **F7**), and then become more continuous and dense (e.g., Fig. **F6**). No evidence for current reworking of cohesive mats (e.g., roll-up structures of Simonson and Carney, 1999) was observed in the cores, but given the bathyal depth at which these sediments accumulated, this is not surprising. Further examination of OAE1a samples (pristine, not impregnated with blue epoxy as in this study) using a scanning electron microscope would be beneficial to understanding the origin of these laminae, perhaps providing conclusive evidence for mat development (i.e., preserved remains of mat-building organisms in life position) (Schieber, 1999).

Surface-grazing organisms or bioturbative mixing could have produced discontinuities in the mat. Observations of modern samples of submarine mats show them to contain a limited indigenous meiofauna of foraminifers and nematodes (Grant, 1991). Leckie et al. (2002) suspect that the smaller planktonic foraminifers associated with OAEs might have been bacterial grazers. But as discussed above, there was no direct evidence of foraminifers within the OAE1a interval on the Shatsky Rise. Discontinuities could also be a product of the geometry and size of the bacterial mats. Direct submarine observations of seasonally developed bacterial mats from the floor of the Santa Barbara Basin show them to occur as patches a few centimeters to meters in scale (Grant, 1991). Photographs indicate that they grade laterally into burrowed dysaerobic sediment (Grant, 1991). Thus, the net product of these variabilities acting through time, especially if mat distributions fluctuate and are overprinted by bioturbation, could be mostly wispy textures. On the Shatsky Rise, the flattened and stringy clay-rich patches in the OAE1a wispy facies (Fig. **F7**) could be fecal in origin. In modern deepwater mats the filamentous bacterial sheaths can bind sediment, including fecal pellets and microfossils, to form a spongy texture (Williams and Reimers, 1983). If originally calcareous (nannofossiliferous), such pellets may have been diagenetically diminished during burial and compaction, with only dissolution residues remaining like deflated balloons. “Interrupted” microlaminations were interpreted by Timofeev et al. (1981) as the products of precipitation from an organic mineral hydrogel, producing montmorillonitic clay minerals and organic seams, strands, or lenses that mimic lamination. Finally, the wispy textures may be fundamentally inherent to mat environments rather than a grazing or pelletal phenomenon, in that such structures are even reported in Archaean carbonaceous cherts where bioturbation and pelletization are not options for their formation (Walsh and Lowe, 1999). Thus, these wispy and discontinuous textures may be of multiple origins. There is evidence for bioturbation in all but the most densely laminated sections, suggesting that anoxia was periodic. Laminated sediments would only survive in the most severe periods of anoxia. Higher

in the Site 1207 OAE1a section, where the laminations become more continuous, the presence of whole fish fossils suggests more pronounced anoxia. The structure of these well-defined laminations in the upper OAE1a at Site 1207 is a function of variations in the density of organic matter, which could represent seasonal fluctuations in organic matter accumulation.

The OAE1a intervals at Sites 1207 and 1213 are ~600 km apart, suggesting that some of the differences between the sections may be attributed to latitudinal variability in oceanic productivity. Furthermore, Site 1207 on the Northern High is estimated to have been at a shallower depth (1.3 km) than sites on the Southern High (e.g., 2.8 km at Site 1213) during deposition of the OAE1a interval (Bralower, Premoli Silva, Malone, et al., 2002). This depth difference could be significant in terms of their relative positions with respect to the carbonate compensation depth (CCD) (Bralower, Premoli Silva, Malone, et al., 2002). Because of the less than perfect recovery of the OAE1a interval (30%–50%), it is difficult to determine whether observed differences between the sections at Sites 1207 and 1213 have been made on truly representative or biased sample sets.

Site 463 Organic-Rich Intervals

There are three organic-rich intervals at Site 463, described as having abrupt bases and gradational tops (Dean et al., 1981). The nature of the organic material recovered at Site 463 is similar to that from the Shatsky Rise (Bralower, Premoli Silva, Malone, et al., 2002). There are several detailed studies of the organic material at Site 463. Timofeev and Bogolyubova (1981) describe granular sapropelic (algal) material similar to the globular (round, <30 µm) material observed at Shatsky, as well as structureless organic–sediment mixtures that they call sapro-collinite. They also term "peculiar" the strandlike to bandlike texture that imparts the horizontal texture (not lamination) to the sediment. The few organic-rich sedimentary rocks from Site 463 examined here (Table T1) are radiolarian porcellanites to claystones with globular (round, <30 µm) to stringy discontinuous organic matter similar in texture to that observed on Shatsky Rise. Petrographic differences between the Shatsky and Site 463 OAE1a intervals found during this study (Table T1) include locally significant replacement of radiolarians by pyrite (Fig. F8) and late-stage replacement by Fe-stained calcite.

F8. Samples from Site 463, p. 23.

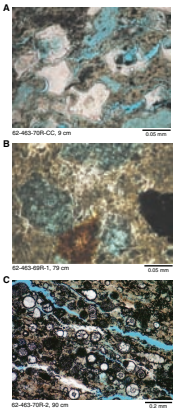

Volcaniclastics Associated with the OAE1a

Overview

OAEs have been variously linked to volcanism. Vogt (1989) suggested that enhanced spreading rates and higher heat flow at the mid-ocean ridges would have warmed ocean bottom waters, eventually resulting in higher productivity. Alternatively, warmer bottom waters may have originated in marginal seas flooded during sea level rise bought about by increased ridge volumes associated with rapid spreading (Arthur et al., 1987). In the Pacific realm, the linkage is also manifested in the close association of the OAE1a with volcanic ash beds (Dean et al., 1984; Sliter 1989, 1999) and the close temporal linkage of the OAE1a to the large pulse (superplume?) of off-ridge mafic volcanic activity that created the Ontong Java and Manihiki Plateaus (Fig. F2) (Larson, 1991b; Larson and Erba, 1999; Tarduno et al., 1991).

The inferences are that the volcaniclastic intervals would have been produced by eruption of these large igneous provinces. However, the OAEs are present on what were then submerged topographic highs (Sliter, 1989) that would have been isolated from direct submarine ash input. This means that the ash must have either been supplied through the water column by air fall or that the ash would have been produced by volcanic centers that were active on each of the highs.

Several questions arise as to the origin of the volcaniclastic intervals associated with the OAE1a on the Shatsky Rise and elsewhere in the Pacific:

Was the ash far traveled or locally derived?
Was the source spectacularly large mafic volcanic events on the Ontong Java Plateau (OJP), felsic arc-related volcanic eruptions, or local mafic volcanism on the Shatsky Rise?
If local, was the volcanic debris pyroclastic, hydroclastic, or epiclastic in origin?
Were there multiple sources of ash?
Did the nature of the source or sources change through time?

There are three possible sources: (1) a magmatic arc to the east; (2) OJP volcanism; and/or (3) volcanism on the Shatsky Rise. Each of these sources might have supplied texturally and compositionally distinct volcanic debris. Deciphering the origin of these ash beds is made more complex because of their intense alteration, including dissolution of glass and mineral grains and precipitation of authigenic phases. However, blue-dyed epoxy impregnation of primary and secondary pores allows for the recognition of textural attributes of the debris (e.g., Fig. **F5**) that shed some light on their composition (mafic to felsic) and likely origin (epiclastic, hydroclastic, or pyroclastic). The feasibility of each source is discussed below.

Magmatic Arc Source

The Aptian is associated with higher rates of seafloor spreading (e.g., Larson, 1991a, 1991b), which implies that rates of subduction and subduction-related magmatism should have also increased around the paleo-Pacific during this time period. Paleogeographic reconstructions place the Shatsky Rise in the equatorial central Pacific, which limits possible source volcanoes to the Central American or northern South American magmatic arcs, which today are the main source of ash in the equatorial central Pacific (Fisher and Schminke, 1984). Far-traveled ash from arc eruptions would have likely consisted of silicic bubble-wall shards and highly to moderately vesiculated glass, similar to that which accumulated in the Cenozoic section as the Shatsky Rise traveled closer to Asian arc sources (**Gadley and Marsaglia,** this volume). These textures were not dominant in the OAE1a-related ash intervals, so an arc-related source seems improbable.

Ontong Java Plateau Source

Early drilling on the OJP suggested that it formed rapidly during the early Aptian (Tarduno et al., 1991). Thanks to ODP Leg 192 (Mahoney, Fitton, Wallace, et al., 2001; Mahoney et al., 2001), more is now known about the basement and cover rocks of the OJP. Biostratigraphic and geochronologic data from this leg and other studies of outcropping

equivalents indicate the plateau was produced in a brief magmatic pulse at ~120 Ma (Mahoney et al., 2001). Shipboard scientists concluded that the plateau was shallow in the Aptian, but other data suggest that it was produced by submarine eruptions (Roberge et al., 2003). At Site 1183 on the OJP (Mahoney, Fitton, Wallace, et al., 2001), 2 m of volcaniclastic turbidite sands consisting of partly glassy basaltic rock fragments and altered brown blocky to moderately vesicular glass shards were recovered above pillowed basalt flows.

Mafic volcanic centers are not known to produce much air fall ash, but Tarduno et al. (1991) suggest that formation of the OJP would have produced "exceptional eruption of ash." They believe this ash is present at Site 167 on a topographic high northeast of the OJP. More recently, Ingle and Coffin hypothesized that submarine basaltic magmatism on the OJP was the product of an extraterrestrial bolide impact that also contributed to the formation of the OAE1a (Coffin and Ingle, 2003; Ingle and Coffin, 2003, 2004). Such an event would also likely first produce pyroclastic ejecta, possibly glassy spherules, then induce voluminous eruptions and production of more pyroclastics.

As shown by biostratigraphic studies (e.g., Erba, 1994), the OAE1a interval slightly postdates the OJP-building event. Thus an OJP source can only be called upon for the ash beds that directly underlie the OAE1a intervals. These ash beds are very altered and mainly consist of birefringent clay (smectite) with traces of plagioclase feldspar. The alteration has obscured any textural information that might have linked them to an OJP. A more parsimonious interpretation is that they were produced by proximal eruptions on the Shatsky Rise.

Local Source

Elsewhere in the western Pacific Ocean, including the Mid-Pacific Mountains, an extensive mid-Cretaceous magmatic event is associated with widespread seamount production and intrusive complexes (Schlanger et al., 1981). This magmatism is thought to have been induced by the Ontong Java event (Tarduno et al., 1991). Previous workers have interpreted the ash beds at Site 463 to be a mixture of epiclastic and pyroclastic debris (Dean et al., 1984); admixed shallow-water fauna led Vallier and Jefferson (1981) and Timofeev et al. (1981) to propose that the source of the volcaniclastic material was a volcanic island. The composition of the alteration products led most to believe that the ash was mafic; however, some proposed a felsic to alkalic component (Hein and Vanek, 1981; Mélières et al., 1981). My observations of thin sections from several tuffaceous intervals at Site 463 (Fig. F8) support a mafic source of volcaniclastic debris above and below the OAE1a horizon. Such a local origin is also plausible for the tuffaceous beds on the Shatsky Rise.

Shatsky Rise is a large (1200 km × 400 km) volcanic plateau that rapidly formed in association with a complex oceanic ridge-ridge-ridge triple junction during the Jurassic–Early Cretaceous (Sager et al., 1988; Nakanishi et al., 1999). Basement drilling has been unsuccessful and there are many unresolved questions as to the origin of the rise (Bralower, Premoli Silva, Malone, et al., 2002; Sager et al., 1988; Nakanishi et al., 1999). Previous workers have seen no evidence for Cretaceous volcanism on the Shatsky Rise associated with the Ontong Java event at 120 Ma (Nakanishi et al., 1999). However, diabase sills intruded into Berriasian sedimentary rocks at Site 1213 (Bralower, Pre-

moli Silva, Malone, et al., 2002) indicate post-Berriasian magmatism on the Southern High dated by Mahoney et al. (2005) at ~144 Ma.

The distribution of ash on the Shatsky Rise, above and below the OAE1a interval, is similar to that observed at Site 463. The ash intervals that occur below the OAE1a interval on the Shatsky Rise are texturally indeterminate (discussed above) but contain no relict microlitic or tachylitic debris, just some vague vesicular textures. In contrast, the ash beds above the OAE1a interval at Site 1207 consist of a mixture of altered blocky to slightly vesicular vitric components of likely hydroclastic origin and epiclastic debris. The epiclastic volcanic grains are subangular to well rounded, include microlitic and tachylitic fragments, and are associated with glauconite (Figs. F5, F6). The microlitic textures and presence of tachylite suggest that these fragments were derived from more slowly cooled (subaerial) basalt flows (see discussion of mafic fragment types in Marsaglia, 1992, 1993). These results suggest that there was a subaerially exposed volcanic edifice on the Northern High soon after OAE1a deposition. Undated rudist- and coral-bearing shallow-marine limestones were recovered from the Southern High, but these could be as old as Jurassic (Sager et al., 1999).

Glauconite is significant as it is generally thought to be produced in modern middle-shelf (50 m) to upper-slope (450 m) environments where sediment accumulation is slow but in ancient systems may have formed in much shallower water (Chafetz and Reid, 2000). At Site 1207, glauconite appears to have been transported along with the epiclastic volcanic debris. Elsewhere in the Pacific, glauconite has been described in the shallow cover sequences of seamounts (e.g., Paleocene at Site 432 on Nintoku Seamount by Marsaglia et al., 1999). Jeans et al. (2000) describe Aptian–Albian glauconitic deposits that formed by the replacement of mafic volcaniclastic sand/silt in marine settings near the island and massif volcanic centers that formed in response to rifting and extension in the North Sea.

As mentioned previously, the OAE1a interval occurs during a period of eustatic sea level rise (Bralower et al., 1993). Thus, the sandy glauconitic and epiclastic beds cannot be attributed to eustatically driven shelf exposure whereby sand was transported into deeper water. Shelf development must instead be linked to volcanic topography. The limitation of the glauconite to directly above the OAE1a interval indicates that, once formed, the topographic highs responsible for these sediments must have then rapidly deepened, perhaps as a response to thermal subsidence compounded by the effects of rising sea level.

SUMMARY AND CONCLUSIONS: A MODEL TO EXPLAIN SHATSKY APTIAN EVENTS

The petrographic and petrologic observations made in this study support the following model. The large-scale submarine volcanism documented across the Pacific at ~120 Ma is now suggested to have affected the Shatsky Rise as well. On the Shatsky Rise, there is a pulse of ash input just prior to the deposition of the OAE1a interval. Its alteration makes its origin somewhat indeterminable; it may have been a direct product of OJP eruptions or, more likely, an indirect product via reactivation of the older volcanic edifices on the rise. Intrusion-related uplift associated with this magmatic rejuvenation may account for the pre-OAE1a submarine unconformities at Sites 1213 and 1214 on the South-

ern High. Alternatively, the hiatus/unconformity could have been produced by scouring of the ridge by deep ocean currents or an impact-related tsunami. There is no evidence for subaerial exposure. Very poor recovery across this interval precludes a more detailed analysis. As suggested by several workers (e.g., Leckie et al., 2002; Larson and Erba, 1999) this Pacific-wide period of submarine volcanism likely increased productivity via iron fertilization. Higher productivity led to enhanced accumulation of organic matter. The organic-rich interval was widespread and developed bacterial mats. Eventually, these volcanic centers built up above sea level, evolving into subaerial volcanoes. Emergence cut off the source of iron, and productivity dramatically declined. The exposed volcanic highs and associated shallow shelf areas then shed a mix of hydroclastic (blocky), epiclastic, and glauconitic debris into deeper water. The epiclastic debris is mostly microlitic and locally tachylitic, suggesting that source lavas cooled slowly, as would be expected in a subaerial setting. Rounding of the epiclastic debris is consistent with transport in a beach setting or possibly a high-energy shelf. The glauconite is a diagenetic replacement of the volcanic debris after it was carried out onto the adjacent shelf. No shallow-water bioclastic debris was observed in these units, but this may be a diagenetic overprint. Alternatively, the "young" island volcanoes may not have had time to develop reef systems. The time frame involved with this interval (tuffaceous and organic-rich intervals) is relatively short, on the order of 1 m.y., which would be consistent with the time frame needed for the rejuvenation and then subsidence of the volcanic centers. This story, although best told through the stratigraphic section on the Shatsky Rise, is also represented in the Mid-Pacific Mountains at Site 463.

ACKNOWLEDGMENTS

This research used samples and/or data provided by the Ocean Drilling Program (ODP). ODP is sponsored by the U.S. National Science Foundation (NSF) and participating countries under management of Joint Oceanographic Institutions (JOI), Inc. Funding for this research was provided by JOI and California State University Northridge.

REFERENCES

Arthur, M.A., Kump, L., Dean, W., and Larson, R., 1991. Superplume? Supergreenhouse? *Eos, Trans. Am. Geophys. Union,* 72:301.

Arthur, M.A., Schlanger, S.O., and Jenkyns, H.C., 1987. The Cenomanian–Turonian oceanic anoxic event, II. Palaeoceanographic controls on organic-matter production and preservation. *In* Brooks, J., and Fleet, A.J. (Eds.), *Marine Petroleum Source Rocks*. Geol. Soc. Spec. Publ., 26:401–420.

Bralower, T.J., Arthur, M.A., Leckie, R.M., Sliter, W.V., Allard, D.J., and Schlanger, S.O., 1994. Timing and paleoceanography of oceanic dysoxia/anoxia in the late Barremian to early Aptian. *Palaios,* 9:335–369.

Bralower, T.J., Premoli Silva, I., Malone, M.J., et al., 2002. *Proc. ODP, Init. Repts.,* 198 [CD-ROM]. Available from: Ocean Drilling Program, Texas A&M University, College Station TX 77845-9547, USA.

Bralower, T.J., Sliter, W.V., Arthur, M.A., Leckie, R.M., Allard, D.J., and Schlanger, S.O., 1993. Dysoxic/anoxic episodes in the Aptian–Albian (Early Cretaceous). *In* Pringle, M.S., Sager, W.W., Sliter, W.V., and Stein, S. (Eds.), *The Mesozoic Pacific: Geology, Tectonics, and Volcanism*. Geophys. Monogr., 77:5–37.

Bralower, T.J., and Thierstein, H.R., 1984. Organic carbon and metal accumulation rates in Holocene and mid-Cretaceous sediments: paleogeographic significance. *In* Brooks, J., and Fleet, A.J. (Eds.), *Marine Petroleum Source Rocks:* Spec. Publ.—Geol. Soc. London, 345–369.

Chafetz, H.S., and Reid, A., 2000. Syndepositional shallow-water precipitation of glauconitic minerals. *Sediment. Geol.,* 136:29–42.

Coccioni, R., Erba, E., and Premoli Silva, I., 1992. Barremian–Aptian calcareous plankton biostratigraphy from the Gorgo Cerbara section (Marche, central Italy) and implications for plankton evolution. *Cretaceous Res.,* 13:517–537.

Coffin, M.F., and Ingle, S., 2003. Impact origin for the greater Ontong Java Plateau? Geophysical and geodynamical evidence. *Eos, Trans. Am. Geophys. Union,* 46 (Suppl.):V12B-0576. (Abstract)

Dean, W.E., Claypool, G.E., and Thiede, J., 1981. Origin of organic-carbon-rich mid-Cretaceous limestones, Mid-Pacific Mountains and southern Hess Rise. *In* Thiede, J., Vallier, T.L., et al., *Init. Repts. DSDP,* 62: Washington (U.S. Govt. Printing Office), 877–890.

Dean, W.E., Claypool, G.E., and Thiede, J., 1984. Accumulation of organic matter in Cretaceous oxygen-deficient depositional environments in the central Pacific Ocean. *Org. Geochem.,* 7:39–51.

Erba, E., 1994. Nannofossils and superplumes: the early Aptian "nannoconids crisis." *Paleoceanography,* 9:483–501.

Fisher, R.V., and Schmincke, H.-U., 1984. *Pyroclastic Rocks:* New York (Springer-Verlag).

Grant, C.W., 1991. Distribution of bacterial mats (*Beggiatoa* spp.) in Santa Barbara Basin, California: a modern analog for organic-rich facies of the Monterey Formation [M.S. thesis]. California State Univ., Long Beach.

Hein, J.R., and Vanek, E., 1981. Origin and alteration of volcanic ash and pelagic brown clay, Deep Sea Drilling Project Leg 62, north-central Pacific. *In* Thiede, J., Vallier, T.L., et al., *Init. Repts. DSDP,* 62: Washington (U.S. Govt. Printing Office), 559–569.

Hochuli, P., Menegatti, A.P., Weissert, H., and Erba, E., 1999. High-productivity and cooling episodes in the early Aptian Alpine Tethys. *Geology,* 27:657–660.

Ingle, S., and Coffin, M., 2004. Impact origin of the greater Ontong Java Plateau? *Earth Planet. Sci. Lett.,* 218:123–134.

Ingle, S., and Coffin, M.F., 2003. Impact origin for the greater Ontong Java Plateau? Geochemical and petrologic evidence. *Eos, Trans. Am. Geophys. Union,* 84(46):V12B-0575. (Abstract)

Jeans, C.V., Wray, D.S., Merriman, R.J., and Fisher, M.J., 2000. Volcanogenic clays in Jurassic and Cretaceous strata of England and the North Sea Basin. *Clay Miner.,* 35:25–55.

Larson, R.L., 1991a. Geological consequences of superplumes. *Geology,* 19:963–966.

Larson, R.L., 1991b. Latest pulse of Earth: evidence for a mid-Cretaceous super plume. *Geology,* 19:547–550.

Larson, R.L., and Erba, E., 1999. Onset of the Mid-Cretaceous greenhouse in the Barremian–Aptian: igneous events and the biological, sedimentary and geochemical responses. *Paleoceanography,* 14:663–678.

Larson, R.L., Moberly, R., et al., 1975. *Init. Repts. DSDP,* 32: Washington (U.S. Govt. Printing Office).

Leckie, R.M., Bralower, T.J., and Cashman, R., 2002. Oceanic anoxic events and plankton evolution: biotic response to tectonic forcing during the mid-Cretaceous. *Paleoceanography,* 17:10.1029/2001PA000623.

Mahoney, J.J., Duncan, R.A., Tejada, M.L.G., Sager, W.W., and Bralower, T.J., 2005. Jurassic–Cretaceous boundary age and mid-ocean ridge-type mantle source for Shatsky Rise. *Geology,* 33:185–188.

Mahoney, J.J., Fitton, G., Wallace, P., and the Leg 192 Scientific Party, 2001. ODP Leg 192: basement drilling on the Ontong Java Plateau. *JOIDES J.,* 27(2):2–11.

Mahoney, J.J., Fitton, J.G., Wallace, P.J., et al., 2001. *Proc. ODP, Init. Repts.,* 192 [CD-ROM]. Available from: Ocean Drilling Program, Texas A&M University, College Station, TX 77845-9547 USA.

Marsaglia, K.M., 1992. Petrography and provenance of volcaniclastic sands recovered from the Izu-Bonin arc, Leg 126. *In* Taylor, B., Fujioka, K., et al., *Proc. ODP, Sci. Results,* 126: College Station, TX (Ocean Drilling Program), 139–154.

Marsaglia, K.M., 1993. Basaltic island sand provenance. *In* Johnsson, M.J., and Basu, A. (Eds.), *Processes Controlling the Composition of Clastic Sediments*. Spec. Pap.—Geol. Soc. Am., 284:41–65.

Marsaglia, K.M., Mann, P., Hyatt, R.J., and Olson, H.C., 1999. Evaluating the influence of aseismic ridge subduction and accretion (?) on detrital modes of forearc sandstone: an example form the Kronotsky Peninsula in the Kamchatka forearc. *Lithos,* 46:17–42.

Mélières, F., Deroo, G., and Herbin, J.-P., 1981. Organic-matter-rich and hypersiliceous Aptian sediments from western Mid-Pacific Mountains, Deep Sea Drilling Project Leg 62. *In* Thiede, J., Vallier, T.L., et al., *Init. Repts. DSDP,* 62: Washington (U.S. Govt. Printing Office), 903–915.

Nagel, U., and Schumann, D., 1981. X-ray mineralogy of sediments, Deep Sea Drilling Project 62. *In* Thiede, J., Vallier, T.L., et al., *Init. Repts. DSDP,* 62: Washington (U.S. Govt. Printing Office), 529–535.

Nakanishi, M., Sager, W.W., and Klaus, A., 1999. Magnetic lineations within Shatsky Rise, northwest Pacific Ocean: implications for hot spot–triple junction interaction and oceanic plateau formation. *J. Geophys. Res.,* 104:7539–7556.

Pedersen, T.F., and Calvert, S.E., 1990. Anoxia vs. productivity: what controls the formation of organic-carbon-rich sediments and sedimentary rocks? *AAPG Bull.,* 74:454–466.

Premoli Silva, I., Erba, E., Salvini, G., Locatelli, C., and Verga, D., 1999. Biotic changes in Cretaceous oceanic anoxic events of the Tethys. *J. Foraminiferal Res.,* 29:352–370.

Rateev, M.A., Timofeev, P.P., and Koporulin, V.I., 1981. Clay minerals in Mesozoic and Cenozoic sediments of Deep Sea Drilling Project Leg 62. *In* Thiede, J., Vallier, T.L., et al., *Init. Repts. DSDP,* 62: Washington (U.S. Govt. Printing Office), 537–544.

Roberge, J., White, R., Wallace, P., and Coffin, M., 2003. Anomalous subsidence of the Ontong Java Plateau (ODP Leg 192). *Eos, Trans. Am. Geophys. Union,* 84(46):V12B-0574. (Abstract)

Sager, W.W., Handschumacher, D.W., Hilde, T.W.C., and Bracey, D.R., 1988. Tectonic evolution of the northern Pacific plate and Pacific-Farallon-Izanagi triple junction in the Late Jurassic and Early Cretaceous (M21–M10). *Tectonophysics,* 155:345–364.

Sager, W.W., Kim, J., Klaus, A., Nakanishi, M., and Khankishieva, L.M., 1999. Bathymetry of Shatsky Rise, northwest Pacific Ocean: implications for ocean plateau development at a triple junction. *J. Geophys. Res., [Solid Earth Planets],* 104:7557–7576.

Schieber, J., 1999. Microbial mats in terrigenous clastics: the challenge of identification in the rock record. *Palaios,* 14:3–12.

Schieber, J., 2003. Simple gifts and buried treasures—implications of fining bioturbation and erosion surfaces in black shales. *Sediment. Rec.,* 1:4–8.

Schlanger, S.O., Jenkyns, H.C., and Premoli-Silva, I., 1981. Volcanism and vertical tectonics in the Pacific Basin related to global Cretaceous transgressions. *Earth Planet. Sci. Lett.,* 52:435–449.

Shipboard Scientific Party, 1981. Site 463: western Mid-Pacific Mountains. *In* Thiede, J., Vallier, T.L., et al., *Init. Repts. DSDP,* 62: Washington (U.S. Govt. Printing Office), 33–156.

Simonson, B.M., and Carney, K.E., 1999. Roll-up structures: evidence of in situ microbial mats in late Archaen deep shelf environments. *Palaios,* 14:13–24.

Sliter, W.V., 1989. Aptian anoxia in the Pacific Basin. *Geology,* 17:909–912.

Sliter, W.V., 1999. Cretaceous planktic foraminiferal biostratigraphy of the Calera limestone, northern California, USA. *J. Foraminiferal Res.,* 29:318–329.

Stow, D.A.V., Huc, A.-Y., and Bertrand, P., 2001. Depositional processes of black shales in deep water. *Mar. Pet. Geol.,* 18:491–498.

Tarduno, J.A., Sliter, W.V., Kroenke, L., Leckie, M., Mayer, H., Mahoney, J.J., Musgrave, R., Storey, M., and Winterer, E.L., 1991. Rapid formation of Ontong Java Plateau by Aptian mantle plume volcanism. *Science,* 254:399–403.

Timofeev, P.P., and Bogolyubova, L.I., 1981. Cretaceous sapropelic deposits of Deep Sea Drilling Project Sites 463, 465, and 466. *In* Thiede, J., Vallier, T.L., et al., *Init. Repts. DSDP,* 62: Washington (U.S. Govt. Printing Office), 891–901.

Timofeev, P.P., Renngarten, N.V., and Eremeev, V.V., 1981. Lithologic-genetic characteristics of sediments in a section at Site 463, Deep Sea Drilling Project Leg 62. *In* Thiede, J., Vallier, T.L., et al., *Init. Repts. DSDP,* 62: Washington (U.S. Govt. Printing Office), 607–615.

Vallier, T.L., and Jefferson, W.S., 1981. Volcanogenic sediments from Hess Rise and the Mid-Pacific Mountains, Deep Sea Drilling Project Leg 62. *In* Thiede, J., Vallier, T.L., et al., *Init. Repts. DSDP,* 62: Washington (U.S. Govt. Printing Office), 545–557.

Vogt, P.R., 1989. Volcanogenic upwelling of anoxic, nutrient-rich water: a possible factor in carbonate-bank/reef demise and benthic faunal extinctions? *Geol. Soc. Am. Bull.,* 101:1225–1245.

Walsh, M.M., and Lowe, D.R., 1999. Modes of accumulation of carbonaceous matter in the early Archaen: a petrographic and geochemical study of the carbonaceous cherts of the Swaziland Supergroup. *In* Lowe, D.R., and Byerly, G.R. (Eds.), *Geologic Evolution of the Barberton Greenstone Belt, South Africa*. Spec. Pap.—Geol. Soc. Am., 329:115–132.

Williams, L.A., and Reimers, C., 1983. Role of bacterial mats in oxygen-deficient marine basins and coastal upwelling regimes; preliminary report. *Geology,* 11:267–269.

Figure F1. Location map for Leg 198 sites on the Shatsky Rise. The rise is ~1500 km long and 500 km wide. The rise comprises three prominent highs (Southern, Central, and Northern), all of which were tested during Leg 198. Sites 1207, 1213, and 1214 are the focus of this study in that they contained early Aptian organic-rich shales and tuffaceous sedimentary rocks. Perspective is viewed from the south looking north. From Bralower, Premoli Silva, Malone, et al. (2002).

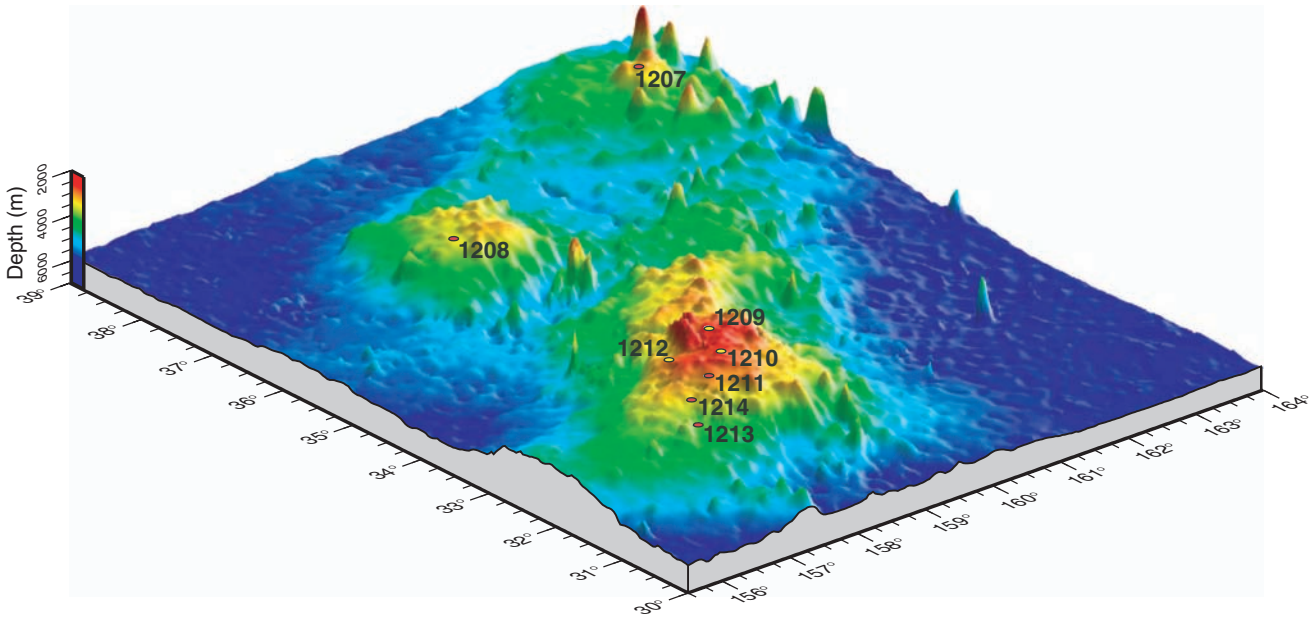

Figure F2. Location of topographic highs in the western Pacific. Deep Sea Drilling Project Site 463 is located in the Mid-Pacific Mountains. Modified from Bralower, Premoli Silva, Malone, et al. (2002).

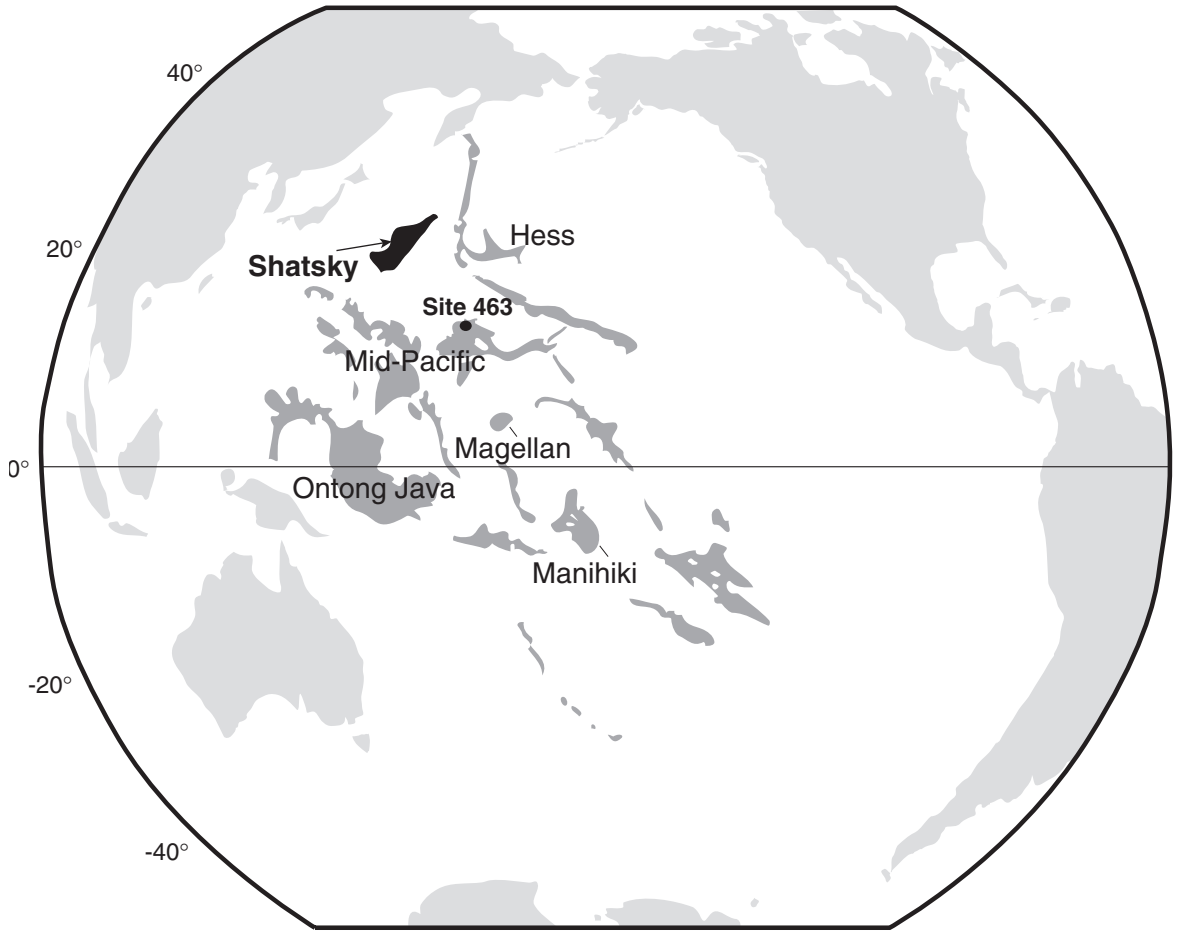

Figure F3. Series of core photographs from Bralower, Premoli Silva, Malone, et al. (2002) showing OAE1a core sections and sample intervals (red). Vertical scale is in cm. Note that core photographs are of archive halves, whereas samples were taken from the working halves of cores. The position of the red rectangles, representing sample intervals, were slightly shifted, if necessary, to correspond to the exact archive half of the sample analyzed.

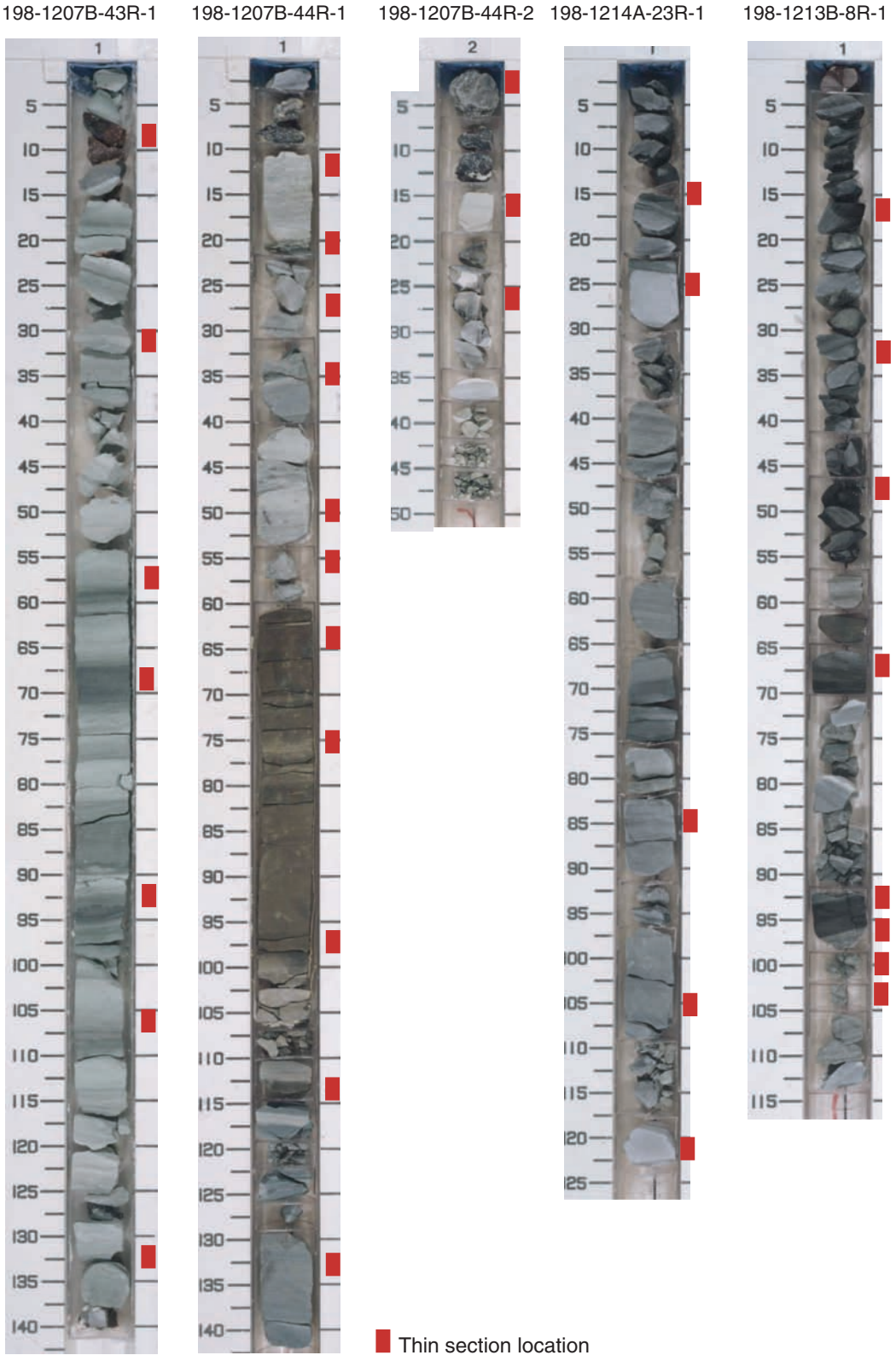

Figure F4. A scanned image of thin sections from the OAE1a interval in Hole 1207B. Prior to thin section preparation, billets were impregnated with blue-dyed epoxy. Encasing epoxy is darker blue, whereas the shade of blue within the rock sample is a function of the relative percentage of microporosity. Some samples are highly porous (e.g., nannofossil chalk in Sample 198-1207B-44R-2, 15 cm) whereas others are nonporous (e.g., partly chertified calcareous porcellanite in Sample 198-1207B-44R-2, 1 cm, and brown organic-rich shales). Contacts between nonporous and porous lithologies within the thin section are emphasized (e.g., Sample 198-1207B-44R-1, 114 cm). In some instances these porosity contrasts define burrows (e.g., Samples 198-1207B-44R-1, 47 cm, and 44R-1, 54 cm). Lighter areas in the brown organic-rich samples (Samples 198-1207B-44R-1, 62 cm, 44R-1, 74 cm, and 44R-1, 96 cm) are clay or porcellanite. Note gradational contact in Sample 198-1207B-44R-1, 96 cm (lighter on top).

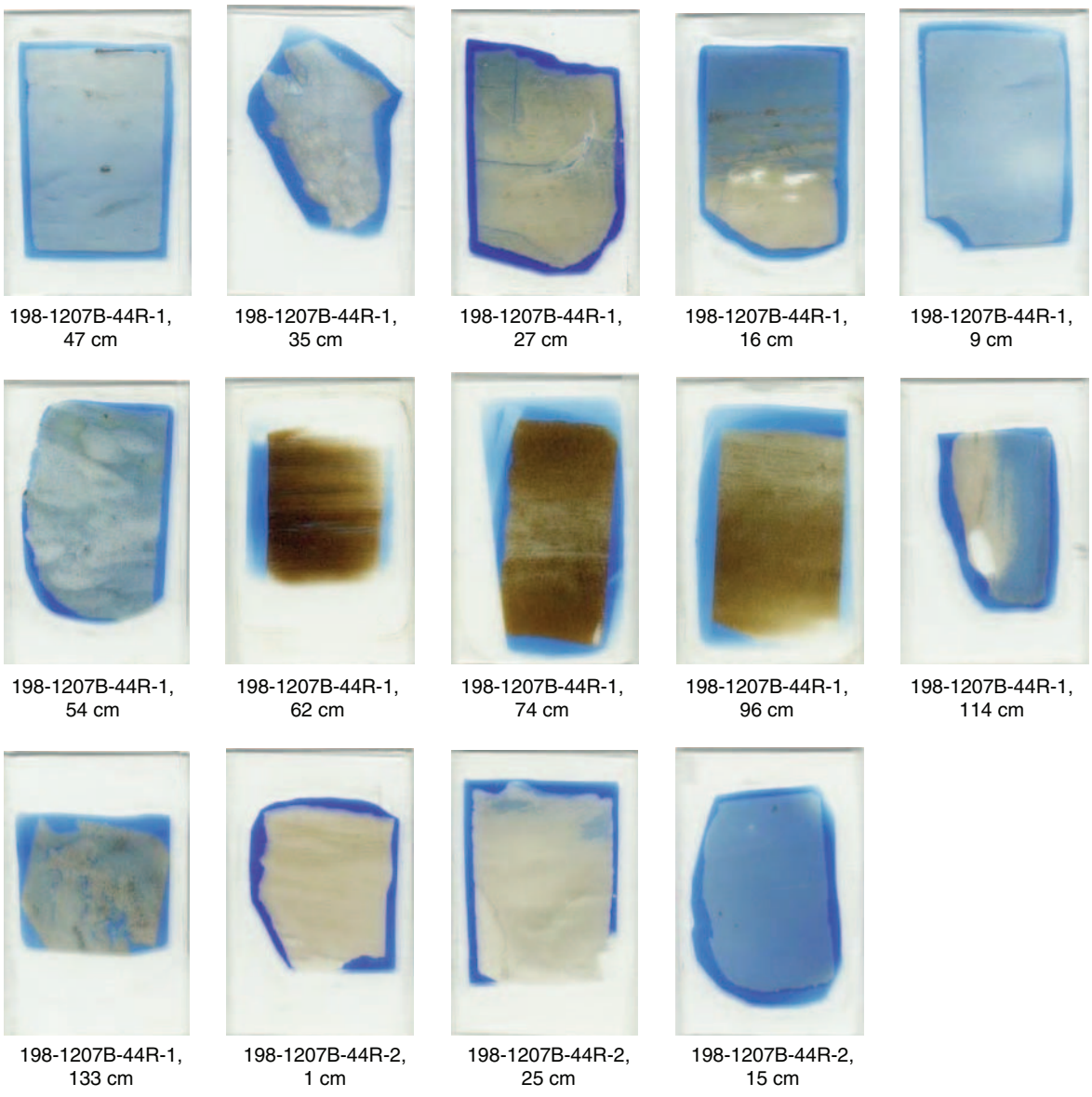

Figure F5. Pictured on the left are core photographs with sample intervals and scales as in Figure F3, p. 18. Stars highlight intervals corresponding to photomicrographs on the right (all in plane-polarized light). **A.** Darker rounded grains are microporous microlitic fragments, whereas light blue grains represent dissolved glassy (?) debris. Rounded green glauconite is present in upper left. **B.** Black glassy (tachylite) fragment in center contains partly dissolved plagioclase laths. **C.** Grains consist of a mixture of secondary pores after blocky to vesicular glass (blue), tachylitic glass (black), and glass altered to clay minerals (brown). White crystals are secondary zeolites. Grains are outlined by authigenic clay mineral cements. **D.** Lower magnification view showing grain-supported nature of this very fine grained volcaniclastic sandstone. Note white rectangular plagioclase crystals and sparse green glauconite grains. Blue porosity is dominantly secondary in origin.

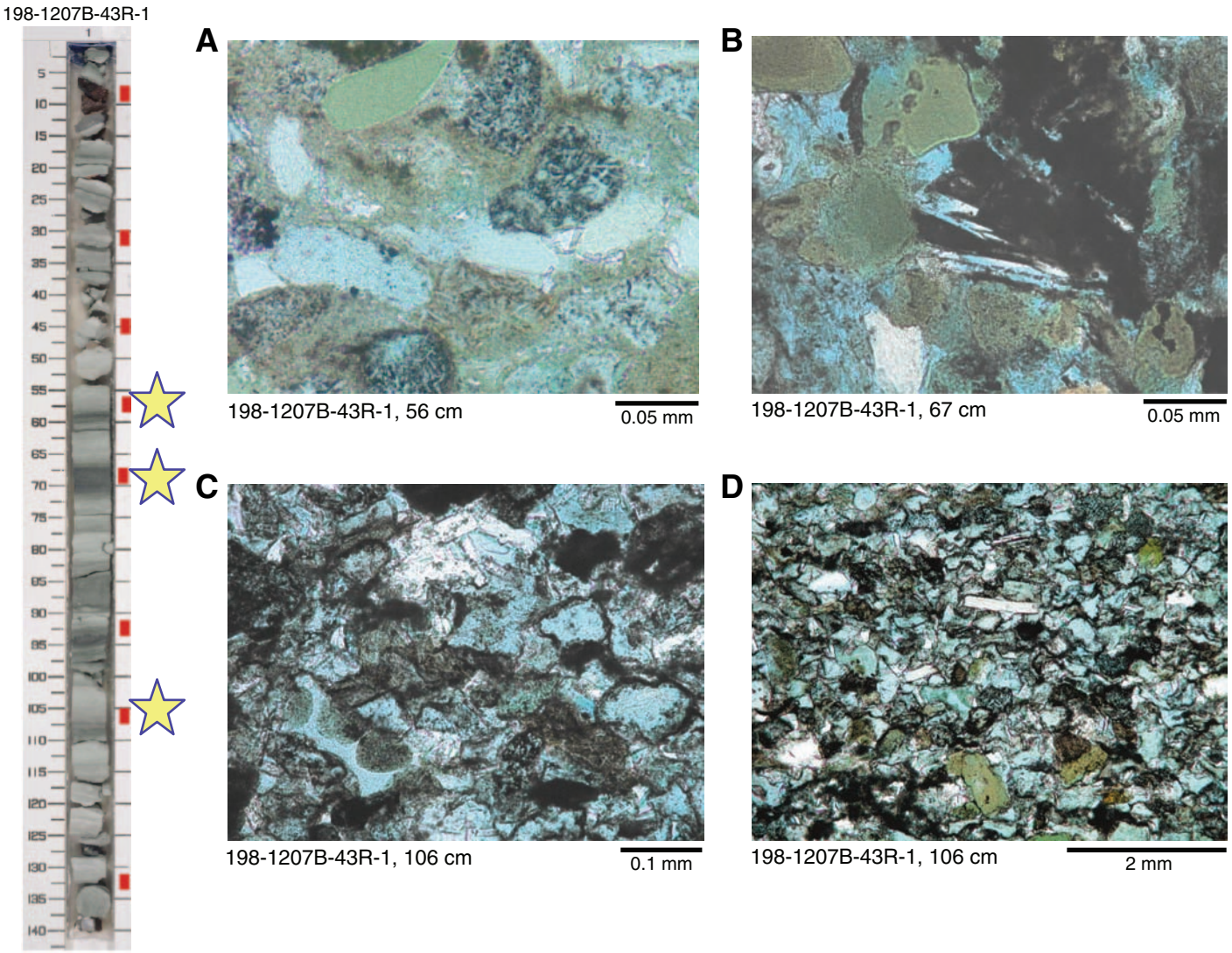

Figure F6. Pictured on the left is a core photograph with sample intervals and scale as in Figure F3, p. 18. Stars highlight intervals corresponding to photomicrographs on the right (all in plane-polarized light). **A.** Main components in this tuff are blocky vitric fragments that are white because they have been altered to zeolites. Note rounded microlitic grain in left center. **B.** Laminated organic-rich shale is a close-up of the central portion of D. **C.** Small brown globular structures (example circled) can be seen in the matrix of this organic-rich radiolarian porcellanite. White circular features are altered radiolarians. **D.** Laminated structure in organic-rich interval exhibits blue, epoxy-filled fractures that are products of sample shrinkage during thin section preparation. White streak in center and blob in lower left are phosphatic fish debris.

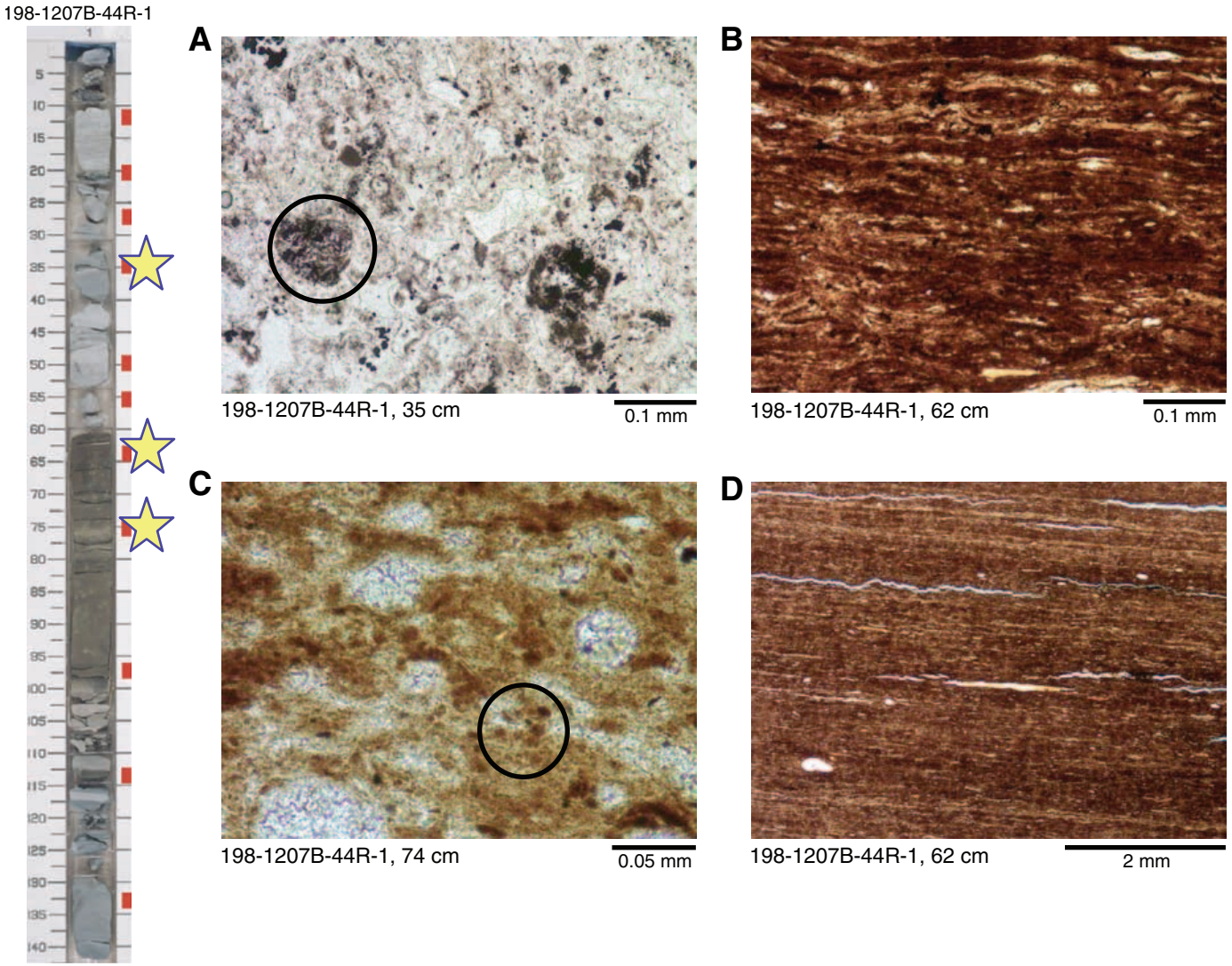

Figure F7. Pictured on the left is a core photograph with sample intervals and scale as in Figure F3, p. 18. Stars highlight intervals corresponding to photomicrographs on the right (all in plane-polarized light except C, which is with nicols crossed). **A.** Wispy to peletal texture in organic-rich chert. White areas are distorted (compacted) radiolarians infilled by chalcedony. **B.** Bioturbated contact between organic-rich porcellanite (light) and organic-rich shale (dark). Note discrete burrows in porcellanite infilled by organic-rich shale (circled in photomicrograph) and similar distribution of radiolarians (white circular features) throughout both lithologies. **C.** Radiolarian sparite. Circular features are radiolarians completely infilled and enveloped by large poikilotopic calcite crystals (relative extinction marked by shades of gray). **D.** Close-up of radial bioturbation textures (tan linear streaks) in organic-rich shale.

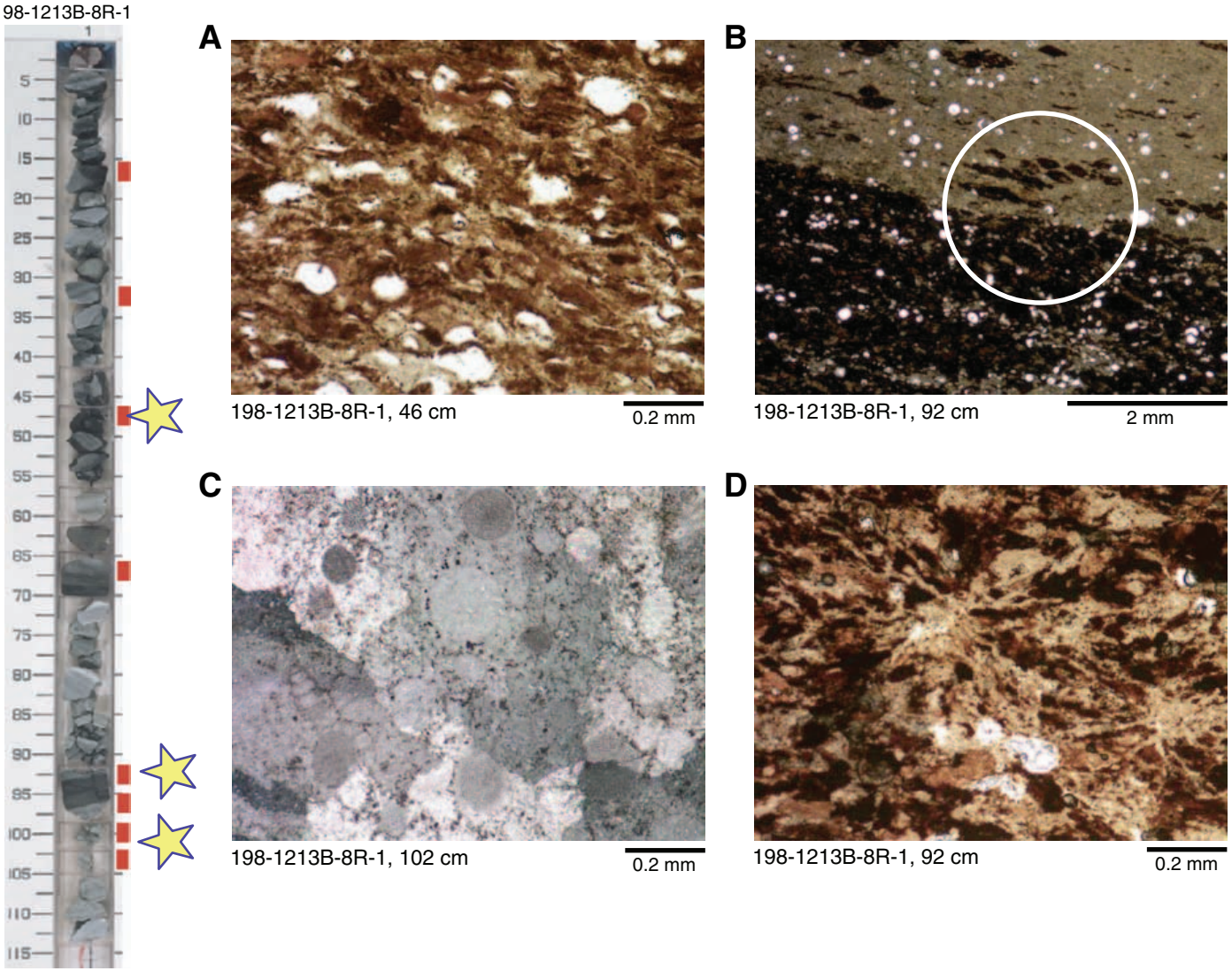

Figure F8. Photomicrographs of samples from Site 463 (all in plane-polarized light). **A.** White fragments are moderately to slightly vesicular blocky glass replaced by zeolite in an altered tuff. **B.** Altered tuff with clay matrix (brown) and microporous volcanic lithic fragments (blue). **C.** Radiolarite where delicate radiolarians have been replaced by pyrite (black) and infilled by carbonate (white).

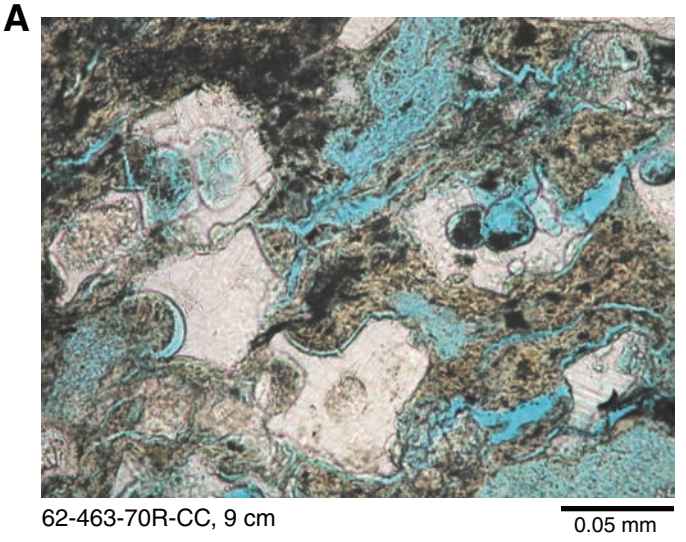

Table T1. Petrographic summary of thin sections from ODP Sites 1207, 1213, 1214, and DSDP Site 463. (Continued on next five pages.)

Core, section, interval (cm)	Depth (mbsf)	XRD	Biogenic components						Matrix				
									Detrital		Diagenetic		
			Foraminifer	Nannofossil	Ostracode	Radiolarian	Fish debris	Organic Matter	Clay	Silt	Clay	Opal-CT	Carbonate
198-1207B-													
43R-1, 8			R	—	—	A	R	—	—	—	—	C	C
43R-1, 30			R	A	—	R	R	—	—	—	?	—	A
43R-1, 56		**	—	—	—	—	R	—	A	—	—	A	A
43R-1, 67		**	C	—	R	R	C	—	A	—	—	—	A
43R-1, 91		**	R	A	—	R	R	—	—	—	A	—	—
43R-1, 105		**	R	C	—	R	—	—	R	—	—	—	—
43R-1, 132			R	A	R	C	—	—	?	—	—	A	?
44R-1, 9			R	A	R	A	R	—	—	—	—	—	—
44R-1, 16		**	R	A	R	R	R	—	—	—	C	?	—
44R-1, 27			—	C	—	A	R	—	R?	—	—	R?	—
44R-1, 35		**	—	—	—	R	—	—	—	—	A	—	—
44R-1, 47			R	A	R	C	R	—	—	—	—	A	—
44R-1, 54		**	—	—	—	A	R	—	C	—	?	—	—
44R-1, 62		**	—	—	—	R	—	C	A	R	—	—	—
44R-1, 74		**	—	—	—	C	R	C	C	R	—	—	—
44R-1, 96		**	—	—	—	C	R	C	A	R	—	A	—
44R-1, 114		**	—	—	—	C	—	—	—	—	A	A	—
44R-1, 133		**	R	—	—	C	R	—	—	—	A	—	—
44R-2, 1			R	A	—	R	R	—	—	—	—	C	—
44R-2, 15			R	A	R	—	R	—	—	—	—	—	—
44R-2, 25			C	A	—	—	R	—	—	—	—	R	R
198-1213B-													
8R-1, 16		**	R	—	—	C	—	R	C	R	—	A	—
8R-1, 32		**	R	—	—	C	R	—	—	—	—	A	—
8R-1, 46			—	—	—	C	R	C	—	—	—	—	—
8R-1, 66		**	—	—	—	C	R	C	A	—	—	A	—
8R-1, 92		**	—	—	—	C	R	C	A	R	—	A	—
8R-1, 95		**	—	—	—	R	—	C	A	R	—	A	—
8R-1, 99			—	—	—	A/C	—	—	R	—	—	—	—
8R-1, 102		**	—	—	—	A/C	—	—	R	—	—	—	—
8R-1, 105		**	—	—	—	C	R	R	A	R	—	C	—
198-1214A-													
23R-1, 13A			—	—	—	C	R	R	A	—	—	—	—
23R-1, 13B			R	—	—	C	—	—	C	—	—	A	—
23R-1, 23			—	—	—	A/C	—	—	C	—	—	—	—
23R-1, 84			—	—	—	C	R	—	A	—	—	A	—
23R-1, 104			—	—	—	C	R	—	—	—	—	—	—
23R-1, 120			—	A	—	C	—	—	—	—	—	?	—
62-463-													
69R-1, 69	604.69		—	—	—	R	—	—	A	—	—	—	—
69R-1, 79	604.79		R	—	—	—	—	—	A	—	A	—	—
69R-1, 112	605.12												
70R-1, 104	614.54												
70R-1, 123	614.73												
70R-2, 87	615.87		—	—	—	A	R	C	A	—	—	A	R
70R-2, 90	615.90		—	—	—	A	R	C	—	—	A	—	—
70R-3, 45	616.95												
70R-7, 19	622.69												
70R-7, 34	622.84		—	—	—	C	—	—	A	—	—	—	—
70R-CC, 9	622.95		—	—	—	A	—	—	A	—	—	—	—
70R-CC, 23	623.09												
71R-1, 39	623.39												
71R-1, 126	624.26												
71R-2, 59	625.09												
71R-2, 68	625.18												
71R-4, 77	628.27												

Note: XRD = X-ray diffraction; R = rare (<5%), C = common (5%–30%), A = abundant (>30%), ** = analyzed by XRD. Levels of bioturbation: intense (>50%), moderate (10%–<50%), slight (<10%), and barren (—).

Table T1 (continued).

Core, section, interval (cm)	Depth (mbsf)	XRD	Matrix		Volcanic Debris							Cement	
			Diagenetic		Glass (Lvv)		Microlitic						
			Quartz	Pyrite	Blocky	Vesicular	volcanic lithic	Plagioclase	Lithic tuff	Pellets	Glauconite	Carbonate	Opal-CT
198-1207B-													
43R-1, 8			C	—	—	—	—	—	—	—	R	—	R
43R-1, 30			—	—	—	—	—	—	—	—	—	R	—
43R-1, 56		**	—	—	R	—	R	R		—	C	—	R
43R-1, 67		**	—	—	—	—	C	R	R	—	C	—	—
43R-1, 91		**	—	—	A	—	R	R	—	—	R	—	—
43R-1, 105		**	—	—	A	R	A	R	—	—	C	—	—
43R-1, 132			A	—	—	—	—	—	—	—	—	—	—
44R-1, 9			—	—	—	—	—	—	—	—	—	C	—
44R-1, 16		**	—	—	—	?	—	—	—	R	—	R	R
44R-1, 27			—	—	—	—	—	—	—	R?	—	—	—
44R-1, 35		**	—	C	A	C	R	—	—	—	—	—	—
44R-1, 47			—	—	—	?	—	—	—	R	—	R	C
44R-1, 54		**	—	—	—	—	—	—	—	—	—	—	C
44R-1, 62		**	—	—	—	—	—	—	—	?	—	—	—
44R-1, 74		**	—	—	—	—	—	—	—	—	—	—	C
44R-1, 96		**	—	—	—	—	—	—	—	—	—	—	C
44R-1, 114		**	—	—	—	—	—	R	—	—	—	—	R
44R-1, 133		**	—	—	—	R?	—	R	—	?	—	—	—
44R-2, 1			—	C	—	?	—	—	—	—	—	R	—
44R-2, 15			—	R	—	—	—	—	—	—	—	R	—
44R-2, 25			A	—	—	—	—	—	—	—	—	C	—
198-1213B-													
8R-1, 16		**	—	—	—	—	—	—	—	—	—	—	—
8R-1, 32		**	—	C	A	—	—	R	—	—	—	—	R
8R-1, 46			C	R	—	—	—	—	—	C	—	—	—
8R-1, 66		**	—	R	—	—	—	—	—	—	—	—	R
8R-1, 92		**	—	—	—	—	—	—	—	—	—	—	R
8R-1, 95		**	—	—	R	—	—	R	—	R/C	—	—	C
8R-1, 99			—	—	R	—	—	R	—	—	—	A	—
8R-1, 102		**	—	—	R	—	—	R	—	—	—	A	—
8R-1, 105		**	—	R	—	—	—	—	—	—	—	—	R
198-1214A-													
23R-1, 13A			—	R	—	—	—	—	—	—	—	—	—
23R-1, 13B			—	—	—	—	—	—	—	—	—	—	R
23R-1, 23			—	—	—	—	—	—	—	—	—	A	—
23R-1, 84			—	—	?	—	—	—	—	—	—	—	C
23R-1, 104			—	—	—	—	—	—	—	—	—	—	R
23R-1, 120			—	—	?	—	—	—	—	R?	—	—	—
62-463-													
69R-1, 69	604.69		—	—	A	R	R	—	—	—	—	R	—
69R-1, 79	604.79		—	—	C	R	C	R	—	—	—	—	—
69R-1, 112	605.12												
70R-1, 104	614.54												
70R-1, 123	614.73												
70R-2, 87	615.87		—	—	—	—	—	—	—	—	—	R	C
70R-2, 90	615.90		—	—	—	—	—	—	—	—	—	C	R
70R-3, 45	616.95												
70R-7, 19	622.69												
70R-7, 34	622.84		—	—	C	C	—	—	—	—	—	A	—
70R-CC, 9	622.95		—	—	C	C	—	—	—	—	—	C	—
70R-CC, 23	623.09												
71R-1, 39	623.39												
71R-1, 126	624.26												
71R-2, 59	625.09												
71R-2, 68	625.18												
71R-4, 77	628.27												

Table T1 (continued).

Core, section, interval (cm)	Depth (mbsf)	XRD	Cement					Porosity					
								Primary			Secondary		
			Chalcedony	Barite	Clay	Pyrite	Zeolite	Within Matrix	Radiolarian/ Foraminifer	Interparticle cement	Radiolarian	Foraminifer	Opal-CT
198-1207B-													
43R-1, 8			R	—	—	R	—	R	—	—	R	—	—
43R-1, 30			R	R?	R	—	—	C	—	—	R	—	—
43R-1, 56		**	R	R	—	—	—	C	—	—	C	—	R
43R-1, 67		**	—	R	—	—	R	—	—	R	—	—	—
43R-1, 91		**	—	R	—	—	R	R	—	—	—	—	—
43R-1, 105		**	—	—	—	—	R	—	—	C	—	—	—
43R-1, 132			R	—	—	R	—	R/A	—	—	—	—	—
44R-1, 9			—	—	—	R	—	—	—	—	—	—	—
44R-1, 16		**	R	R	—	R	—	C	—	—	—	—	—
44R-1, 27			C	—	—	R	—	—	R	—	R	—	—
44R-1, 35		**	—	—	—	—	—	—	—	—	—	—	—
44R-1, 47			R	—	—	R	—	R	—	—	R	R	—
44R-1, 54		**	C	—	—	R	—	C	C	—	R	—	—
44R-1, 62		**	—	—	—	R	R	—	R	—	—	—	—
44R-1, 74		**	C	—	—	R	—	R	R	—	—	—	—
44R-1, 96		**	C	—	—	R	—	—	—	—	—	—	—
44R-1, 114		**	R	—	—	R	—	A?	—	—	R	—	—
44R-1, 133		**	R	—	—	C	C	—	R	—	—	—	—
44R-2, 1			R	—	—	C	—	—	—	—	R	—	—
44R-2, 15			—	R	—	R	—	C	R	—	R	—	—
44R-2, 25			R	R	—	—	—	R	—	—	—	—	—
198-1213B-													
8R-1, 16		**	C	—	—	R	—	—	—	—	—	—	—
8R-1, 32		**	C	—	—	R	R	—	—	—	—	—	—
8R-1, 46			C	—	—	—	—	—	—	—	—	—	—
8R-1, 66		**	—	—	—	—	—	—	R	—	—	—	—
8R-1, 92		**	C	—	—	—	—	R	—	—	—	—	—
8R-1, 95		**	R	—	—	—	R	—	R	—	R	—	—
8R-1, 99			—	—	—	R	R	C?	—	—	—	—	—
8R-1, 102		**	—	—	—	R	R	C?	—	—	—	—	—
8R-1, 105		**	R			R		C	—	—	—	—	—
198-1214A-													
23R-1, 13A			—	—	—	—	—	R	R	—	R	—	—
23R-1, 13B			C	—	—	R	—	—	—	—	—	—	—
23R-1, 23			—	R	—	R	R	—	—	—	—	—	—
23R-1, 84			C	—	—	R	—	—	—	—	—	—	—
23R-1, 104			R	—	—	R	—	—	R	—	R	—	—
23R-1, 120			C	—	—	R	—	—	—	—	—	—	—
62-463-													
69R-1, 69	604.69		—	—	—	—	—	—	—	—	—	—	—
69R-1, 79	604.79		—	—	—	—	—	—	—	—	—	—	—
69R-1, 112	605.12												
70R-1, 104	614.54												
70R-1, 123	614.73												
70R-2, 87	615.87		C	—	—	R	—	—	—	—	—	—	—
70R-2, 90	615.90		R	—	—	R	—	—	—	—	—	—	—
70R-3, 45	616.95												
70R-7, 19	622.69												
70R-7, 34	622.84		—	—	—	R	R	—	R	—	—	—	—
70R-CC, 9	622.95		—	—	R	—	A	—	R	—	—	—	—
70R-CC, 23	623.09												
71R-1, 39	623.39												
71R-1, 126	624.26												
71R-2, 59	625.09												
71R-2, 68	625.18												
71R-4, 77	628.27												

Table T1 (continued).

Core, section, interval (cm)	Depth (mbsf)	XRD	Porosity		Diagenesis			
			Secondary		Pyritized Radiolarian/ Foraminifer	Grains replaced by		Calcitized Radiolarian
			Volcanic	Plagioclase		Glauconite	Zeolite	
198-1207B-								
43R-1, 8			—	—	—	—	—	R
43R-1, 30			—	—	—	—	—	R
43R-1, 56		**	C	—	—	—	—	—
43R-1, 67		**	C	—	—	—	—	—
43R-1, 91		**	—	—	R	—	—	—
43R-1, 105		**	A	—	—	R	R	—
43R-1, 132			—	—	—	—	—	—
44R-1, 9			—	—	—	—	—	C
44R-1, 16		**	—	—	R	—	—	R
44R-1, 27			—	—	—	—	—	—
44R-1, 35		**	—	—	—	—	A	—
44R-1, 47			?	—	—	—	—	—
44R-1, 54		**	—	—	—	C	—	—
44R-1, 62		**	—	—	R	—	—	—
44R-1, 74		**	—	—	R	—	—	—
44R-1, 96		**	—	—	R	—	—	—
44R-1, 114		**	—	—	R	—	—	—
44R-1, 133		**	—	—	R	—	—	—
44R-2, 1			?	—	R	—	—	—
44R-2, 15			—	—	—	—	—	—
44R-2, 25			—	—	R	—	—	R
198-1213B-								
8R-1, 16		**	—	—	—	—	—	—
8R-1, 32		**	C	—	—	—	—	—
8R-1, 46			—	—	R	—	—	—
8R-1, 66		**	—	—	R	—	—	—
8R-1, 92		**	—	—	—	—	—	—
8R-1, 95		**	—	—	—	—	—	—
8R-1, 99			—	—	—	—	—	—
8R-1, 102		**	—	—	—	—	—	—
8R-1, 105		**	—	—	—	—	—	—
198-1214A-								
23R-1, 13A			—	—	—	—	—	—
23R-1, 13B			—	—	R	—	—	—
23R-1, 23			—	—	R	—	—	R
23R-1, 84			—	—	—	—	—	—
23R-1, 104			—	—	—	—	—	—
23R-1, 120			—	—	R	—	—	—
62-463-								
69R-1, 69	604.69		—	—	—	—	—	—
69R-1, 79	604.79		R	R	—	—	—	—
69R-1, 112	605.12							
70R-1, 104	614.54							
70R-1, 123	614.73							
70R-2, 87	615.87		—	—	—	—	—	—
70R-2, 90	615.90		—	—	A	—	—	—
70R-3, 45	616.95							
70R-7, 19	622.69							
70R-7, 34	622.84		—	—	—	—	—	—
70R-CC, 9	622.95		—	—	—	—	A	—
70R-CC, 23	623.09							
71R-1, 39	623.39							
71R-1, 126	624.26							
71R-2, 59	625.09							
71R-2, 68	625.18							
71R-4, 77	628.27							

Table T1 (continued).

Core, section, interval (cm)	Depth (mbsf)	XRD	Diagenesis: Silicified Foraminifer	Rock name	Sedimentary structures
198-1207B-					
43R-1, 8			R	Radiolarian chert and porcellanite	Lamination?
43R-1, 30			R	Glauconitic limestone	Lamination
43R-1, 56		**	—	Volcaniclastic glauconitic sandstone/shale and radiolarian porcellanite	Lamination
43R-1, 67		**	—	Glauconitic volcanic sandstone, zeolitic shale, and chalk	Lamination
43R-1, 91		**	—	Volcaniclastic mudstone to chalk	Lamination
43R-1, 105		**	—	Volcaniclastic fine sandstone (lamina)	Lamination
43R-1, 132			R	Siliceous radiolarian chalk to porcellanite	—
44R-1, 9			—	Radiolarian-bearing nannofossil chalk/limestone	—
44R-1, 16		**	—	Chalk/limestone, claystone, and porcellanite	—
44R-1, 27			—	Radiolarite to radiolarian porcellanite	—
44R-1, 35		**	—	Altered fine vitric tuff	—
44R-1, 47			R	Partly silicifed chalk to calcareous porcellanite	—
44R-1, 54		**	—	Radiolarite to radiolarian porcellanite	—
44R-1, 62		**	—	Organic shale	Lamination
44R-1, 74		**	—	Radiolarian organic shale to porcellanite	—
44R-1, 96		**	—	Radiolarian organic shale to porcellanite	—
44R-1, 114		**	—	Radiolarian porcellanite	—
44R-1, 133		**	?	Zeolitic radiolarian claystone	—
44R-2, 1			R	Partly chertified calcareous porcellanite	Wispy laminae
44R-2, 15			—	Nannofossil chalk	—
44R-2, 25			R	Nannofossil-foraminifer chalk, porcellanite, and chert	
198-1213B-					
8R-1, 16		**	—	Porcellanite with organic matter	Lamination
8R-1, 32		**	—	Volcaniclastic mudstone and radiolarian porcellanite	Lamination
8R-1, 46			—	Radiolarian organic chert	Flattening
8R-1, 66		**	—	Radiolarian organic shale	?(burrows)
8R-1, 92		**	—	Radiolarian organic shale to porcellanite	Bedding plane
8R-1, 95		**	—	Porcellanite with volcaniclastic-filled burrow, organic-rich shale	Burrowed bedding plane?
8R-1, 99			—	Carbonate-cemented radiolarite with patchy volcaniclastic mud	—
8R-1, 102		**	—	Carbonate-cemented radiolarite with patchy volcaniclastic mud	—
8R-1, 105		**	—	Radiolarian shale/porcellanite	? Linear burrow?
198-1214A-					
23R-1, 13A			—	Radiolarian shale	—
23R-1, 13B			—	Radiolarian porcellanite to claystone	Vague lamination
23R-1, 23			—	Radiolarian sparite	—
23R-1, 84			—	Radiolarian clayey porcellanite	—
23R-1, 104			—	Radiolarian claystone	—
23R-1, 120			—	Partly silicified chalk/limestone	—
62-463-					
69R-1, 69	604.69		—	Altered volcaniclastic very fine sandstone to mudstone	—
69R-1, 79	604.79		—	Fine volcaniclastic sandstone to mudstone	—
69R-1, 112	605.12			Nannofossil chalk/limestone with Fe stained carbonate and volcaniclastic burrow fill	
70R-1, 104	614.54			Shale with organic matter, radiolarians, and Fe carbonate replacement	
70R-1, 123	614.73			Radiolarian shale with carbonate replacement	
70R-2, 87	615.87		—	Radiolarian porcellanite with organic matter	Lamination
70R-2, 90	615.90		—	Radiolarian claystone and organic porcellanite	Lamination
70R-3, 45	616.95			Radiolarian shale	
70R-7, 19	622.69			Radiolarian limestone to porcellanite	
70R-7, 34	622.84		—	Radiolarian calcareous and volcaniclastic mudstone	Lamination
70R-CC, 9	622.95		—	Volcaniclastic mudstone to very fine sandstone and radiolarian calcareous shale	Lamination
70R-CC, 23	623.09			Radiolarian shale partly replaced by carbonate	
71R-1, 39	623.39			Radiolarian porcellanite	
71R-1, 126	624.26			Shale	
71R-2, 59	625.09			Limestone	
71R-2, 68	625.18			Radiolarian porcellanite	
71R-4, 77	628.27			Nannofossil chalk/limestone	

Table T1 (continued).

Core, section, interval (cm)	Depth (mbsf)	XRD	Bioturbation	Comments
198-1207B-				
43R-1, 8			Slight	
43R-1, 30			Slight	Ghosts of volcanic debris?
43R-1, 56		**	Slight	
43R-1, 67		**	Moderate	
43R-1, 91		**	Slight	
43R-1, 105		**	Moderate	
43R-1, 132			Slight	
44R-1, 9			Moderate	
44R-1, 16		**	Moderate	
44R-1, 27			Moderate	Veins
44R-1, 35		**	Moderate	
44R-1, 47			Slight	
44R-1, 54		**	Intense	
44R-1, 62		**	Moderate	
44R-1, 74		**	Moderate	
44R-1, 96		**	Moderate	
44R-1, 114		**	Slight	
44R-1, 133		**	—	
44R-2, 1			—	
44R-2, 15			—	
44R-2, 25			?	Arched structure defined by opal-CT
198-1213B-				
8R-1, 16		**	Moderate	
8R-1, 32		**	Slight	
8R-1, 46			—	Compaction, whole fish?
8R-1, 66		**	Moderate	
8R-1, 92		**	Moderate to intense?	Whole fish?
8R-1, 95		**	Intense	
8R-1, 99			?	
8R-1, 102		**	?	
8R-1, 105		**	Slight?	
198-1214A-				
23R-1, 13A			Moderate?	
23R-1, 13B			Moderate to slight	
23R-1, 23			Slight?	Carbonate aggraded?
23R-1, 84			Slight	
23R-1, 104			Slight?	
23R-1, 120			Slight	
62-463-				
69R-1, 69	604.69		Slight	
69R-1, 79	604.79		Slight	
69R-1, 112	605.12			
70R-1, 104	614.54			
70R-1, 123	614.73			
70R-2, 87	615.87		?	
70R-2, 90	615.90		Slight	
70R-3, 45	616.95			
70R-7, 19	622.69			
70R-7, 34	622.84		—	
70R-CC, 9	622.95		—	
70R-CC, 23	623.09			
71R-1, 39	623.39			
71R-1, 126	624.26			
71R-2, 59	625.09			
71R-2, 68	625.18			
71R-4, 77	628.27			

Table T2. Bulk and clay fraction mineralogy of selected samples based on X-ray diffraction analyses. (Continued on next page.)

	198-1207B											
Core, Section, Interval (cm):	43R-1, 56	43R-1, 67	43R-1, 91A	43R-1, 105	44R-1, 16	44R-1, 35	44R-1, 54	44R-1, 62	44R-1, 74	44R-1, 96	44R-1, 114	44R-1, 133
Whole rock mineralogy (wt%):												
Quartz	5.6	0.0	0.0	10.7	4.2	0.9	44.4	48.5	25.5	24.3	7.7	1.9
K-feldspar	0.3	0.8	0.9	0.2	0.1	0.7	0.6	1.1	0.4	0.9	0.7	1.4
Plagioclase	2.3	19.3	8.4	0.3	1.1	31.5	0.0	4.4	1.8	2.3	5.2	23.5
Opal-CT	10.6	0.0	0.0	8.3	1.4	0.0	36.4	0.0	50.0	49.2	48.9	0.0
Calcite	57.7	0.1	42.1	64.3	57.7	0.0	0.0	0.0	0.0	0.0	0.0	0.0
Pyrite	0.0	0.0	0.0	0.0	2.6	6.6	5.6	3.1	0.0	0.0	2.7	9.5
Marcasite	0.0	0.0	0.0	0.0	6.1	0.0	0.0	1.6	0.0	0.0	0.3	0.0
Clinoptilolite/heulandite	4.7	53.4	23.9	0.0	13.1	0.0	0.0	7.7	0.0	0.0	11.9	37.6
Halite	3.0	0.0	0.0	1.7	0.0	0.0	0.0	1.6	0.5	0.5	0.0	0.0
Gypsum	0.0	0.8	0.0	0.0	0.5	0.0	3.5	3.0	1.0	0.8	1.4	0.4
Total phyllosilicates	15.7	25.7	24.7	14.4	13.2	60.4	9.4	29.0	20.7	22.1	21.2	25.7
Totals:	100.0	100.0	100.0	100.0	100.0	100.0	100.0	100.0	100.0	100.0	100.0	100.0
Phyllosilicate mineralogy (%):												
R0 M-L I/S (80%–90%S)*	60.5	67.4	74.5	36.7	30.4	96.9	57.6	38.5	24.4	32.9	81.8	97.3
Illite and mica	39.5	32.6	25.5	62.7	68.5	3.0	41.4	60.4	71.6	64.0	16.5	2.6
Kaolinite	0.0	0.0	0.0	0.5	1.0	0.1	0.9	1.0	3.3	2.3	1.2	0.1
Chlorite	0.0	0.0	0.0	0.1	0.2	0.0	0.2	0.1	0.7	0.9	0.5	0.0
Totals:	100.0	100.0	100.0	100.0	100.0	100.0	100.0	100.0	100.0	100.0	100.0	100.0
Summary mineralogy (wt%):												
Quartz	5.6	0.0	0.0	10.7	4.2	0.9	44.4	48.5	25.5	24.3	7.7	1.9
K-feldspar	0.3	0.8	0.9	0.2	0.1	0.7	0.6	1.1	0.4	0.9	0.7	1.4
Plagioclase	2.3	19.3	8.4	0.3	1.1	31.5	0.0	4.4	1.8	2.3	5.2	23.5
Opal-CT	10.6	0.0	0.0	8.3	1.4	0.0	36.4	0.0	50.0	49.2	48.9	0.0
Calcite	57.7	0.1	42.1	64.3	57.7	0.0	0.0	0.0	0.0	0.0	0.0	0.0
Pyrite	0.0	0.0	0.0	0.0	2.6	6.6	5.6	3.1	0.0	0.0	2.7	9.5
Marcasite	0.0	0.0	0.0	0.0	6.1	0.0	0.0	1.6	0.0	0.0	0.3	0.0
Clinoptilolite/heulandite	4.7	53.4	23.9	0.0	13.1	0.0	0.0	7.7	0.0	0.0	11.9	37.6
Halite	3.0	0.0	0.0	1.7	0.0	0.0	0.0	1.6	0.5	0.5	0.0	0.0
Gypsum	0.0	0.8	0.0	0.0	0.5	0.0	3.5	3.0	1.0	0.8	1.4	0.4
R0 M-L I/S (80%–90%S)*	9.5	17.3	18.4	5.3	4.0	58.5	5.4	11.2	5.1	7.3	17.4	25.0
Illite and mica	6.2	8.4	6.3	9.1	9.0	1.8	3.9	17.5	14.8	14.1	3.5	0.7
Kaolinite	0.0	0.0	0.0	0.1	0.1	0.1	0.1	0.3	0.7	0.5	0.3	0.0
Chlorite	0.0	0.0	0.0	0.0	0.0	0.0	0.0	0.0	0.1	0.2	0.1	0.0
Totals:	100.0	100.0	100.0	100.0	100.0	100.0	100.0	100.0	100.0	100.0	100.0	100.0

Note: * = randomly ordered mixed-layer illite/smectite with 80%–90% smectite layers.

Table T2 (continued).

	198-1213B-						
Core, Section, Interval (cm):	8R-1, 16	8R-1, 32	8R-1, 66	8R-1, 92	8R-1, 95	8R-1, 102	8R-1, 105
Whole rock mineralogy (wt%):							
Quartz	21.7	22.2	15.0	9.5	5.9	0.0	7.2
K-feldspar	0.4	0.2	2.3	1.5	0.9	0.4	0.4
Plagioclase	1.1	1.5	3.7	3.9	7.4	1.5	4.2
Opal-CT	57.0	52.2	46.4	52.9	47.9	0.0	47.9
Calcite	0.0	0.0	0.0	0.0	0.0	94.1	0.0
Pyrite	0.5	1.1	1.6	0.3	2.6	0.3	1.8
Marcasite	0.0	0.0	0.0	0.5	0.0	0.0	0.0
Clinoptilolite/heulandite	0.0	3.0	5.1	1.8	17.0	2.8	21.8
Halite	0.0	0.0	0.0	0.0	0.0	0.0	0.0
Gypsum	0.0	0.1	0.5	0.3	0.3	0.0	0.0
Total phyllosilicates	19.3	19.6	25.6	29.3	18.1	0.9	16.6
Totals:	100.0	100.0	100.0	100.0	100.0	100.0	100.0
Phyllosilicate mineralogy (%):							
R0 M-L I/S (80%–90%S)*	17.0	33.7	23.1	32.5	51.1	76.7	46.9
Illite and mica	82.2	63.7	72.2	64.7	46.8	23.3	53.1
Kaolinite	0.3	0.8	1.1	0.7	0.7	0.0	0.0
Chlorite	0.5	1.8	3.6	2.1	1.4	0.0	0.0
Totals:	100.0	100.0	100.0	100.0	100.0	100.0	100.0
Summary mineralogy (wt%):							
Quartz	21.7	22.2	15.0	9.5	5.9	0.0	7.2
K-feldspar	0.4	0.2	2.3	1.5	0.9	0.4	0.4
Plagioclase	1.1	1.5	3.7	3.9	7.4	1.5	4.2
Opal-CT	57.0	52.2	46.4	52.9	47.9	0.0	47.9
Calcite	0.0	0.0	0.0	0.0	0.0	94.1	0.0
Pyrite	0.5	1.1	1.6	0.3	2.6	0.3	1.8
Marcasite	0.0	0.0	0.0	0.5	0.0	0.0	0.0
Clinoptilolite/heulandite	0.0	3.0	5.1	1.8	17.0	2.8	21.8
Halite	0.0	0.0	0.0	0.0	0.0	0.0	0.0
Gypsum	0.0	0.1	0.5	0.3	0.3	0.0	0.0
R0 M-L I/S (80%–90%S)*	3.3	6.6	5.9	9.5	9.2	0.7	7.8
Illite and mica	15.8	12.5	18.5	19.0	8.5	0.2	8.8
Kaolinite	0.1	0.2	0.3	0.2	0.1	0.0	0.0
Chlorite	0.1	0.4	0.9	0.6	0.3	0.0	0.0
Totals:	100.0	100.0	100.0	100.0	100.0	100.0	100.0